

# Objective Determination of Minimum Engine Mapping Requirements for Optimal SI DIVCP Engine Calibration

Peter J. Maloney  
The MathWorks, Inc.

Copyright © 2009 SAE International

## ABSTRACT

In response to marketplace demand for increased engine performance and economy, spark-ignition (SI) engine applications with dual-independent variable cam-phaser actuators (DIVCP) are now commonplace.

In this paper, the minimum number of test measurements required to optimally calibrate the steady-state spark advance and cam-phaser settings of a SI DIVCP engine was determined, using a high-fidelity model of a 2.2L SI DIVCP engine with predictive combustion capability as a basis.

A calibration development process was designed to objectively determine the minimum number of torque vs. spark advance sweeps required for the SI DIVCP engine.

First, Torque production results from calibration tables based on cost-feasible sets of 52, 96, 173, 250, 329, and 406 sweeps were determined. Next, calibration reference tables were developed from an exhaustive data collection process based on 10,000 sweeps. Finally, torque results from the cost-feasible calibrations were compared to the torque results from the exhaustive reference calibrations tables to determine the minimum number of sweeps required to match the results of the exhaustive approach.

## PROBLEM DEFINITION

An objective process was designed, developed, and executed to determine the minimum testing required for the development of optimal calibration tables related to an engine having the architecture shown in Figure 1.

Figure 1 depicts the test-configuration architecture of a typical production SI 2.2L dual overhead cam (DOHC) inline 4-cylinder (I4), throttle-less, naturally aspirated, port fuel-injected engine equipped with DIVCP and continuously variable intake valve lift (CVIVL) actuators to improve engine performance and economy.

Engine testing (or mapping) is required to generate data necessary to determine the optimal settings for its spark advance, intake variable cam-phasing (VCP), and exhaust VCP as a function of operating points defined by engine speed and engine load.

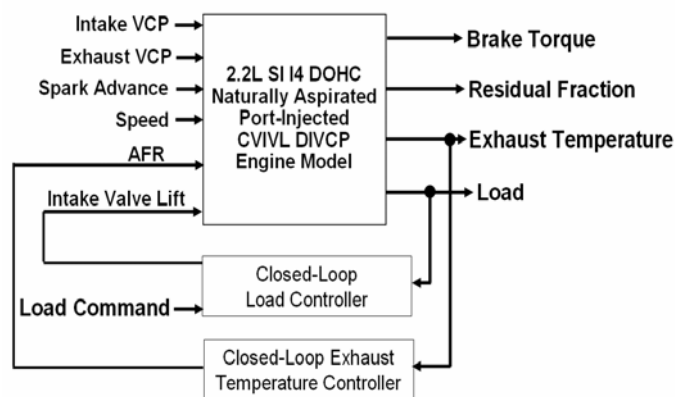


Figure 1. Engine Test Configuration I/O

The commanded and measured engine load variables shown in Figure 1 are defined as normalized cylinder fresh air mass at intake valve close (IVC), which can be inferred by measuring engine fuel flow rate, engine speed, and engine exhaust air-to-fuel (AFR) ratio. Inferred cylinder fresh air mass is normalized to a dimensionless load value by dividing it by the cylinder air mass at piston bottom dead center (BDC), standard temperature and pressure (STP) conditions, and zero engine speed.

During engine testing operations, the test operator typically controls spark advance (S), engine speed (N), Intake VCP (ICP), Exhaust VCP (ECP), and AFR directly. Intake valve lift is then adjusted until a given load (L) command target is reached, and in cases where the engine exhaust temperature is too high for the catalyst and/or engine materials, the AFR is adjusted down (enriched) until the temperature falls to an

acceptable level. The ranges and engineering resolutions of the S, N, L, ICP, and ECP test factors are shown in Table 1.

Factor Name	Minimum Value	Maximum Value	Engineering Resolution
N	500	6000	10 RPM
L	0.15	1	0.002 Ratio
ICP	-5	50	1 Deg Crank Advance
ECP	-5	50	1 Deg Crank Retard
S	0	50	1 Deg BTDC

Table 1. Engine Test Factor Ranges and Resolutions

The ICP and ECP factors in Table 1 have positive values for increasing cam advance and retard with respect to the crankshaft. This means that increasing ICP or ECP will increase valve overlap, which refers to the crank-angle duration where both the intake and exhaust valves are open. High overlap will result in high internal residual burned gases, which will in turn lower combustion temperature and nitrous oxide (NOx) formation in the cylinder with all other factors fixed.

AFR is not included in Table 1 as an engine test factor because it is used to control temperature when and if an over-temperature condition occurs during testing. This paper is concerned with calibration only at engine factor operating points where stoichiometric AFR operation is possible, meaning that AFR is not included explicitly as an independent variable. Non-stoichiometric operating points are not known a-priori for a given engine, but are discovered in the course of testing, and then taken out of the resulting data-set before analysis of the stoichiometric operating region.

Engine calibration operating points are defined in terms of speed N, and load L, and are used to define the independent variable axes of Electronic Control Unit (ECU) calibration lookup tables that store the optimal settings for the other 3 factors – ICP, ECP, and S. Figure 2 below shows the table breakpoint format of the ECU calibration tables used in this paper.

		Engine Speed N (RPM)												
		750	1222	1694	2167	2639	3111	3583	4056	4528	5000			
Engine Load L (ratio)	0.19													
	0.26													
	0.34													
	0.41													
	0.48													
	0.56													
	0.63													
	0.70													
	0.78													
	0.85													

Figure 2. Engine Calibration Table Breakpoints

The work in this paper addressed the following problem statement:

- Determine the minimum number of engine tests required to produce optimal ICP, ECP, and S calibration table settings that maximize brake torque at stoichiometric AFR operation, at the speed and load breakpoints shown in Figure 2, and subject to an upper-bound constraint on internal residual fraction of 20%.

In this paper, a high-fidelity GT-POWER engine model with predictive combustion capability was developed and used as the basis for study, making it necessary to use a residual fraction constraint as a surrogate indication for engine instability, in place of covariance of indicated mean effective pressure (IMEP), which can be measured in a dynamometer laboratory, but which cannot presently be synthesized in engine simulations.

## PROBLEM SOLVING APPROACH

The main approach to solving the problem of optimal calibration development was defined during the fuel crisis of the 1970's[1], and later extended with the addition of Design of Experiments (DoE) methodology and modern Response Surface Modeling (RSM) methods to cover more complex engine applications such as SI DIVCP [2][3].

The good correlation of the RSM models to fitted data and independently measured validation data sets, together with the smooth and physically sensible calibration tables that have resulted from these processes strongly supported the idea that enough testing data had been taken to produce truly optimal calibrations. To date, previous work has not, however, answered the question of how to objectively determine the minimum testing required to produce an optimal calibration for a given engine configuration. Figure 3 shows the process used in this paper to systematically and objectively determine the minimum testing requirements for a SI DIVCP engine configuration.

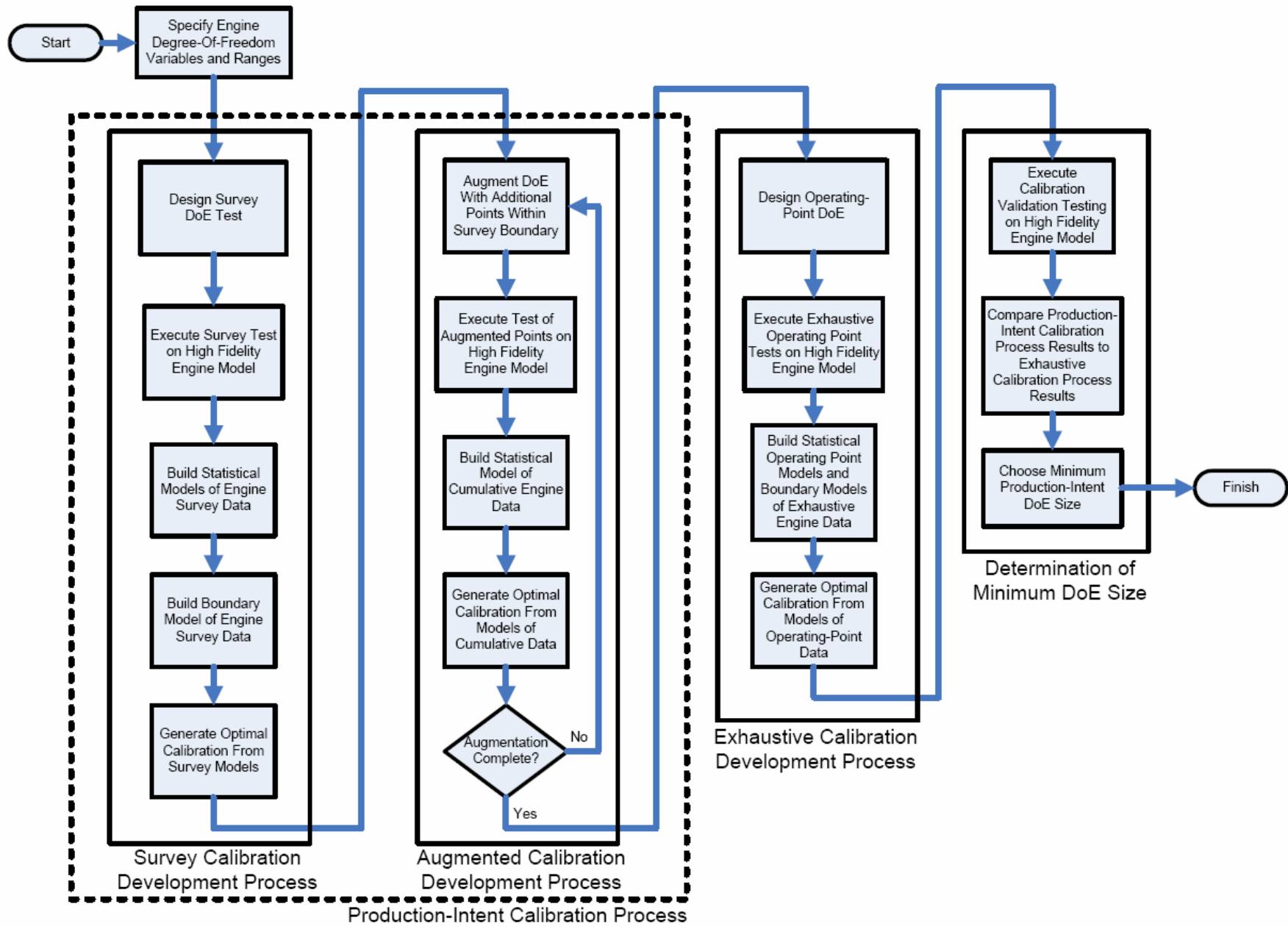


Figure 3. Process for Objective Determination of Minimum Engine Testing Requirements

The major steps of the process shown in Figure 3 are:

- Develop a set of optimal calibrations using a range of DoE experiment sizes with a Production-Intent Calibration Process that is cost-feasible to execute in a dynamometer.
- Develop a reference best-case calibration using an exhaustive testing and modeling process
- Compare the results of the cost-feasible calibrations to the exhaustive reference calibration results to determine the minimum DoE experiment size

### ***Production-Intent Calibration Process***

The Production-Intent Calibration Process shown in Figure 3 represents a cost-feasible testing approach to optimal calibration development from dynamometer-measured data. In this approach, an unconstrained survey test was carried out on the engine factors of Table 1 with a small number of test points to determine the operating envelope of the engine and develop an initial calibration.

The survey test was then augmented progressively with additional test-points in the Augmented Calibration Development Process so that calibrations based on progressively larger test data-sets could be compared.

The Model-Based Calibration Toolbox™ was used throughout the processes shown in Figure 3 to design experiments, produce statistical models of engine responses, and generate optimal calibrations.

### **Survey Test Design**

The Survey Calibration Development Process of Figure 3 was designed to establish the operating envelope of the engine based on the unconstrained variation of the engine factors in Table 1. After unconstrained survey testing, the engine operating envelope was developed based on measured data that met the following criterion:

- Stoichiometric operation was feasible
- Positive brake torque was being generated by the engine

The first step in the Survey Calibration Development Process shown in Figure 3 was to develop an unconstrained experimental design using the engine factors in Table 1. A 32 point Sobol Sequence[4] space-filling DoE was chosen to fill the N, L, ICP, and ECP factor-space defined in Table 1. Spark advance S was not treated as an experimental design variable since it

was treated as a swept variable during testing. A Sobol Sequence design type was chosen because of its ability to support progressive augmentation of DoE points without overlapping test-points and without requiring the starting design to be re-scrambled. A space-filling design type was chosen because it was known from previous work that polynomial models and their associated optimal DoE methods would not sufficiently fit DIVCP engine data.

Figure 4 shows a pair wise plot of the 32 point Sobol Sequence space-fill design. The pair wise plot shows the experimental design factor variations in 2-dimensional slice views.

Due to the importance of defining the maximum and minimum boundaries of the engine operating envelope, together with the fact that 32 space-fill points would not necessarily be sufficient to find the edges of the speed/load envelope of the engine, an additional Sobol Sequence space-fill design of 20 points was added to the survey test at high and low loads.

The exhaust cam phaser was parked (ECP~0) to maximize the load (breathing) potential of the engine. The additional 20 Survey DoE points are shown in Figure 5. The overall Survey DoE test was finalized by merging the 20 point high/low load DoE with the 32 point unconstrained DoE. The final merged Survey design is shown in Figure 6.

### **Survey Test Execution**

After completing the Survey DoE design, the Parallel Computing Toolbox™ was used in conjunction with GT-POWER and Simulink® to test a high-fidelity engine model according to the Survey DoE design, sweeping spark advance S from 0 DegBTDC to 50 BTDC in 5 degree increments at each DoE point. A parallel computing cluster of 16 2.8 GHz Pentium® 4 single-core processor PC machines completed the survey testing in 38 minutes. A Simulink® test-control model was used to provide closed-loop load control via intake valve lift adjustment, to control the engine factors in Table 1, and to adjust AFR for catalyst protection in cases where exhaust temperature exceeded 1200 Degrees Celsius.

### **Statistical Modeling of Survey Test Data**

The measured survey test data were filtered to remove test-points that did not meet the positive torque generation and stoichiometric AFR criterion specified above before statistical modeling was carried out, removing 11 of the original 52 DoE test-points. After filtering, the survey test data were modeled using a two-stage statistical modeling approach, similar to the approaches used in [3]. For each of the 52 DoE test-points defined by N, L, ECP, and ICP, a torque vs. spark regression was performed using the polynomial spline equation form below:

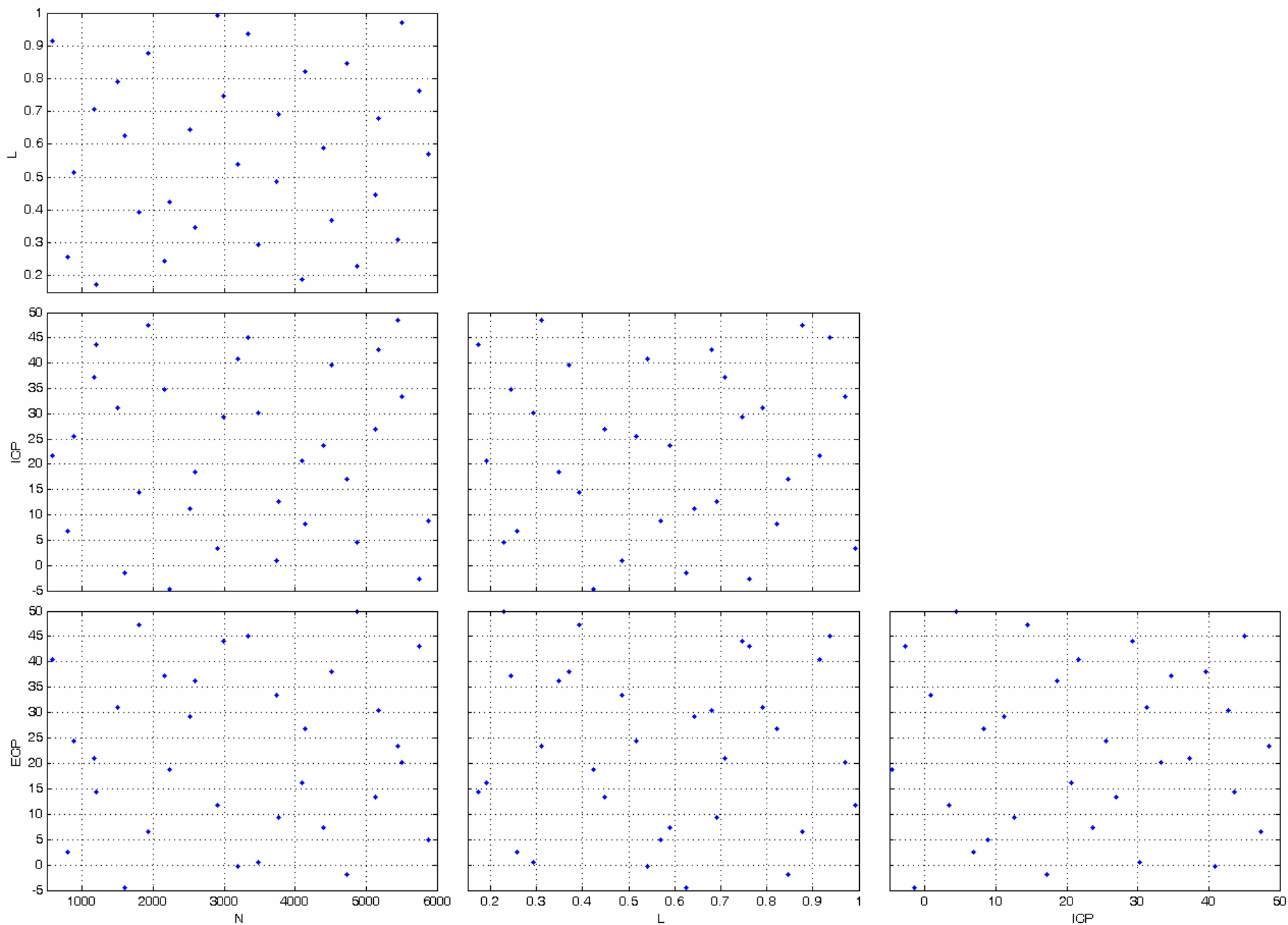


Figure 4. 32 Point Sobol Sequence Space-Fill Survey Test Design of Experiments

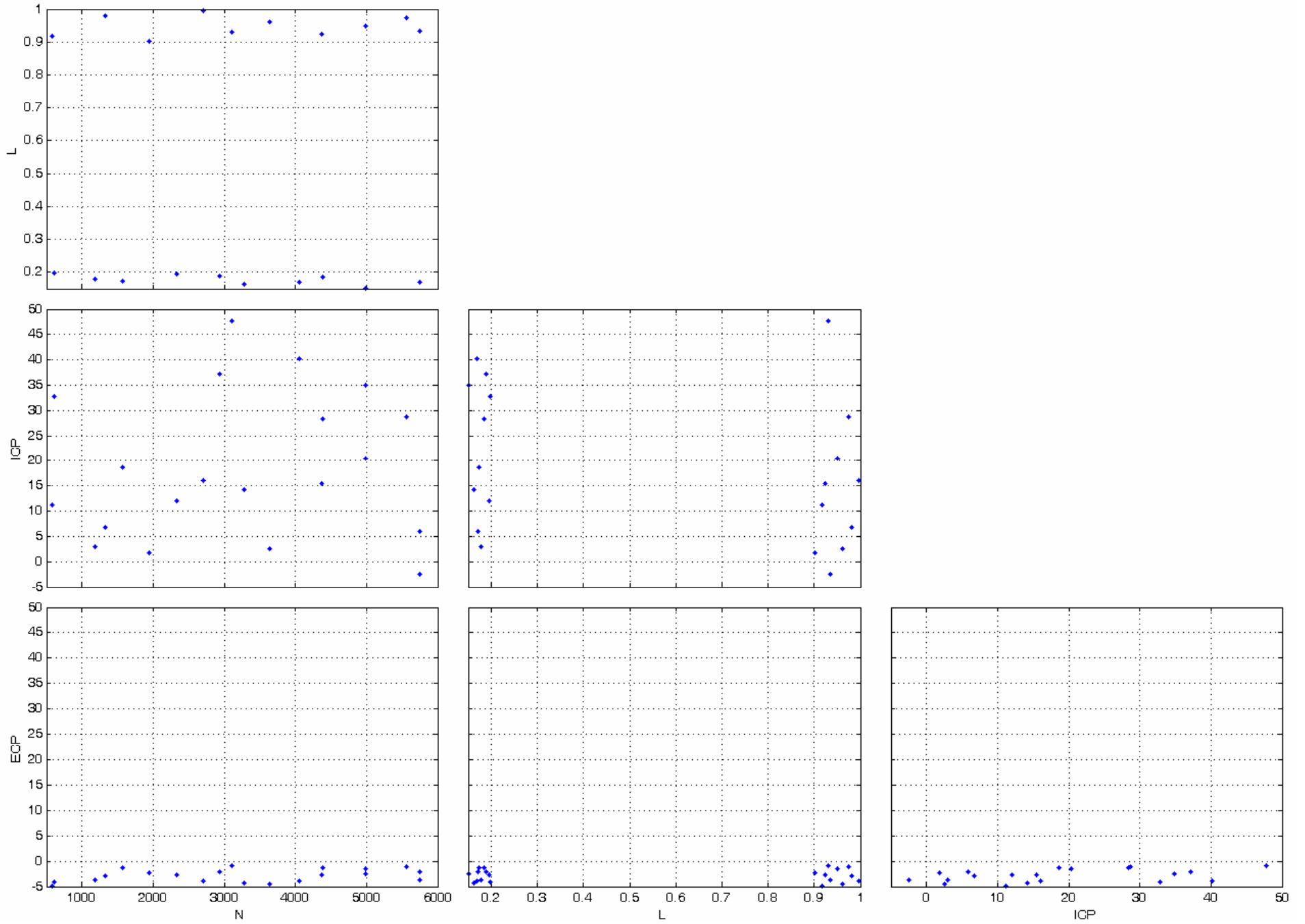


Figure 5. 20 Point High-Load, Low-Load Sobol Sequence Space-Fill Survey Test Augmentation

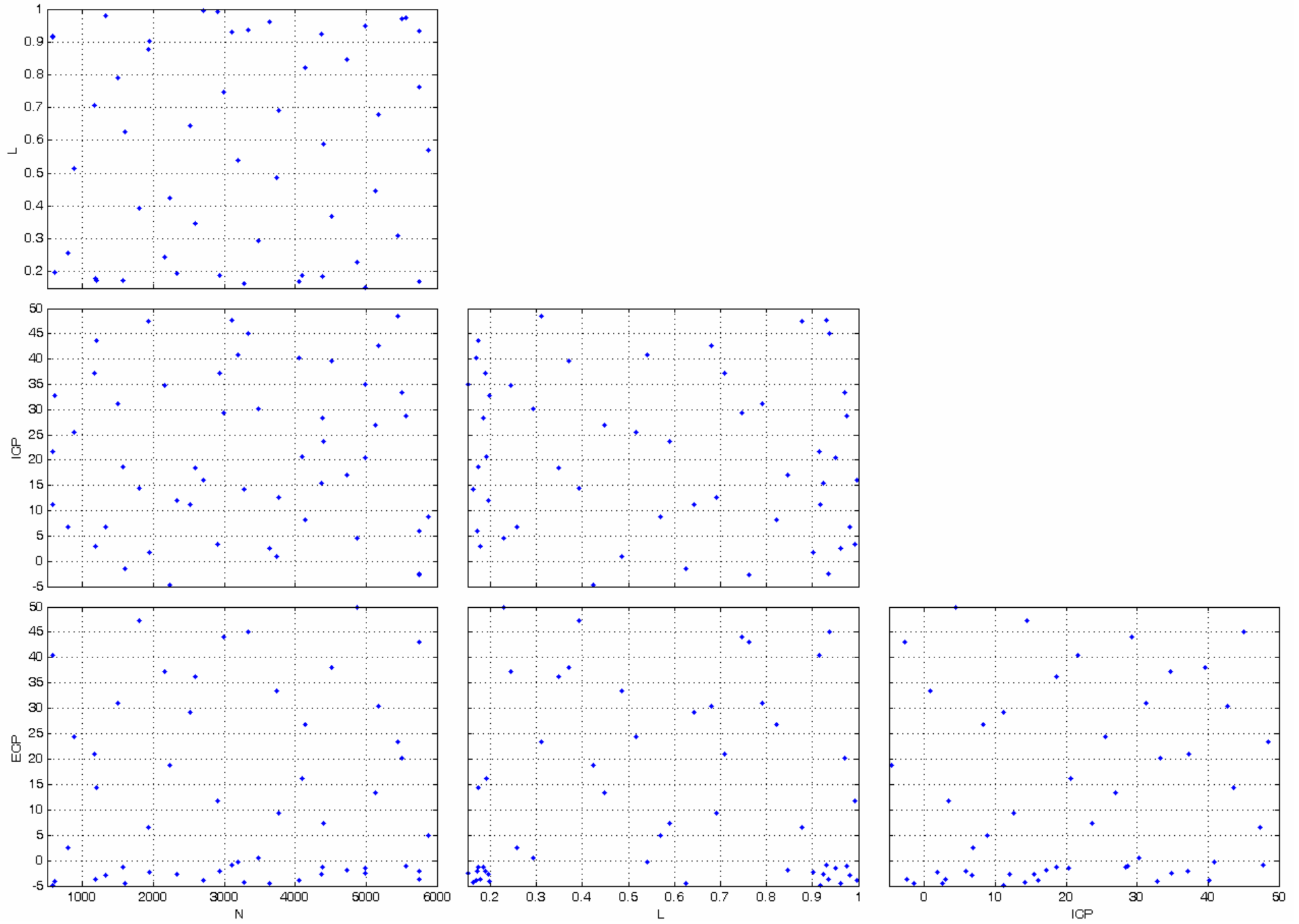


Figure 6. Final Merged 52 Point Sobol Sequence Space-Fill Survey Test Design

$$TQ = \begin{cases} A_0 + A_2(S - A_1)^2, & S \leq A_1 \\ A_0 + A_3(S - A_1)^2, & S > A_1 \end{cases} \quad (\text{EQ. 1})$$

where

$TQ$  is the engine brake torque

$A_0$  is the maximum brake torque as a function of spark advance  $S$

$A_1$  is the location in spark advance of the maximum torque

$A_2$  and  $A_3$  are second-order regression coefficients

Figure 7 shows a graphical representation of the features of a torque vs. spark advance sweep in terms of Equation 1 above. As spark advance is increased throughout its range, torque rises to a maximum, and then falls. Spark knock was not modeled in the GT-POWER engine model used in this paper, so spark advance was not limited as it would be in dynamometer-based testing, where knock-limited spark advance is typically modeled as a separate response and used later in optimization. Equation 1 is a local regression model, meaning that it relates brake torque to spark advance with all other factors ( $N, L, ICP, ECP$ ) held fixed.

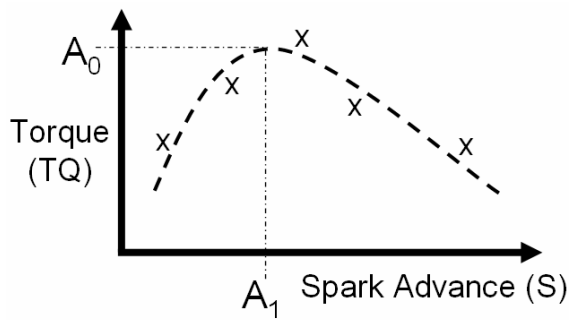


Figure 7. Local Model Characteristics

For each of the 41 torque vs. spark advance local model regressions, a set of regression curve coefficients  $A_{0..3}$  were produced. The regressed coefficients (global models) were in turn regressed against the global test factors  $N, L, ICP,$  and  $ECP$  using a second order Hybrid Radial Basis Function (RBF) model form[5]. A Hybrid RBF form was chosen because of its ability to accurately model fine variations in torque due to tuning effects, without the over-fitting problems associated with other approaches such as high-order polynomials. Figure 8 shows the relationship between global models and global factors.

The radial basis function regressions were fitted using the Regularized Orthogonal Least Squares (ROLS)[5] technique. Eight varieties (Kernels) of RBF types were compared and selected based on the Akaike Information Criteria (AICc) criterion[6] for each of the global models. The ROLS algorithm was initialized with 10 RBF centers, or approximately 25% of the total available data points, in order to achieve a good fit and at the same time avoid over-fitting.

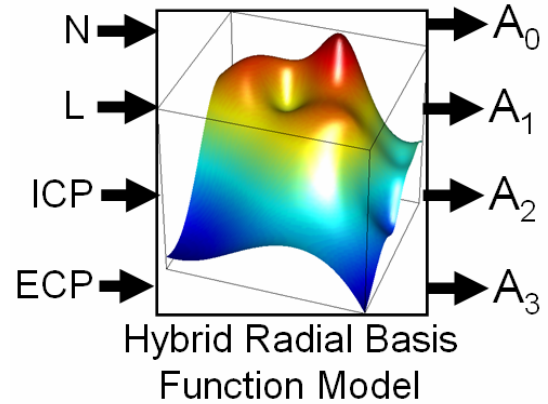


Figure 8. Global Model Form

Table 2 below summarizes the characteristics of the global survey model regressions.

Global Model	Centers	Kernel Type
$A_0$	9	Reciprocal Multiquadric
$A_1$	9	Cubic
$A_2$	10	Logistic
$A_3$	10	Reciprocal Multiquadric

Table 2. Survey Global Model Characteristics

Figure 9 below shows the frequency distribution of the residual differences between predicted and measured torque after removal of outliers, local model fitting, and global model selection. Residual torque values were generally within  $\pm 5$  Nm across 41 spark sweep tests over a total of 273 measurements. Figure 9 includes points that were removed as outliers for model-fitting purposes.

In addition to modeling engine brake torque, the internal residual fraction of burned gas at IVC was modeled as a function of the global variables  $N, L, ECP,$  and  $ICP$  to act

as an indicator of combustion stability in the later optimization phase of work.

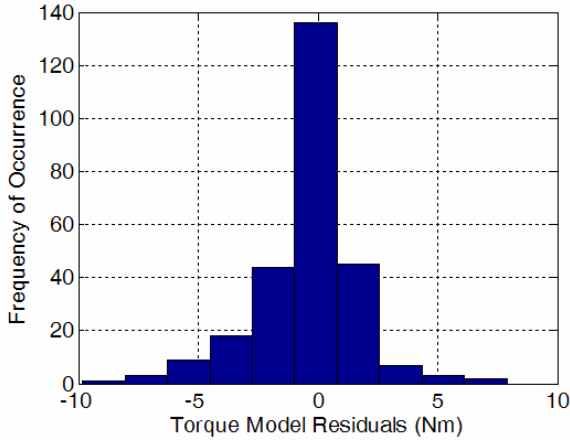


Figure 9. Survey Model Torque Residual Distribution

A cubic RBF with 29 centers was fitted to the measured internal residual corresponding to the maximum torque points in the torque/spark sweeps of the survey. Figure 10 below shows the residual differences between predicted and measured residual fraction, showing that residual fraction has been fitted generally within 1% residual.

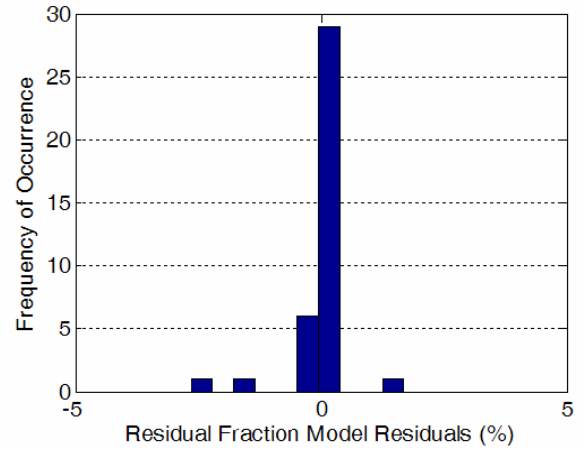


Figure 10. Survey Model Residual Fraction Residual Distribution

### Boundary Modeling of Survey Test Data

It was necessary to develop a model of the boundaries of the factor-space covered by the factors in Table 1 in order to facilitate bounded numerical optimization later in the optimal survey calibration development process. As shown below in the dark areas of Figure 11, a Convex Hull[7] boundary model type was fitted around the N/L

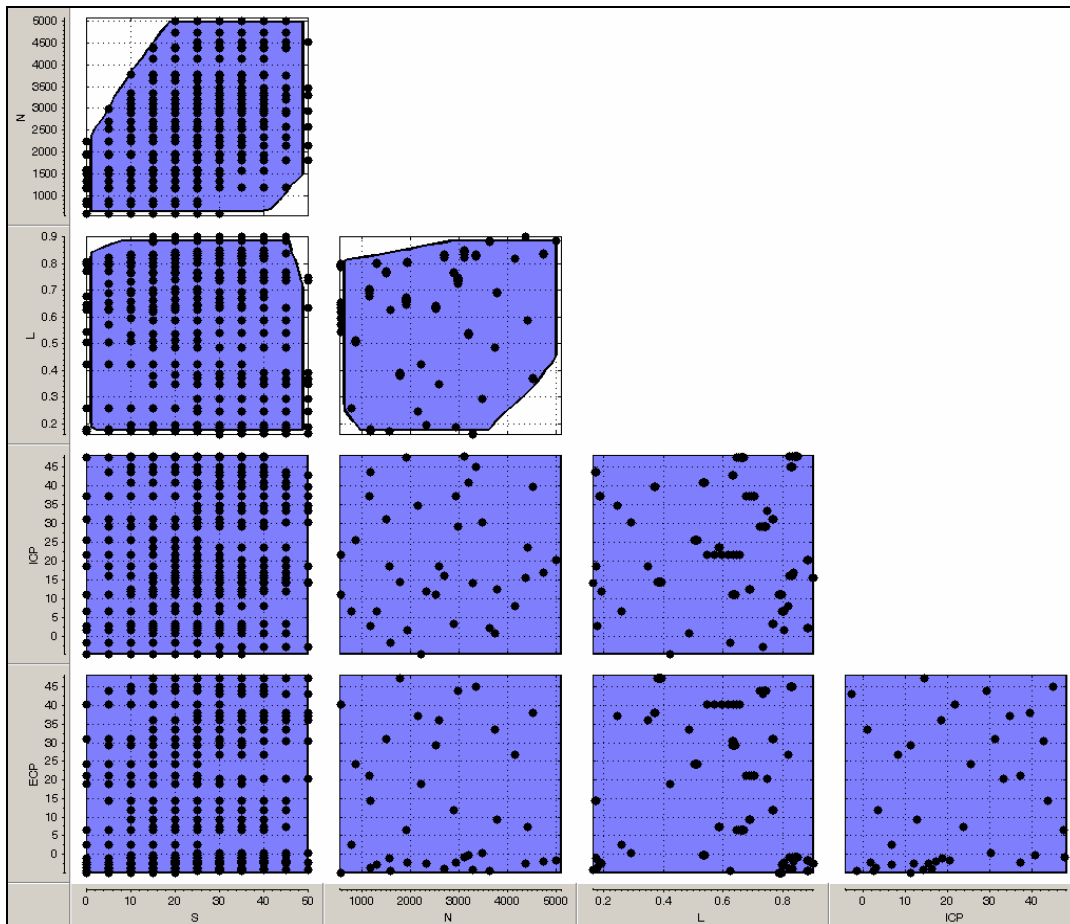


Figure 11. Pairwise View of Convex Hull N/L Boundary, and RBF S Local Boundary

factor-space to account for the natural speed/load operating envelope of the engine, primarily related to the breathing capability of the engine, but also reflecting the region of operation where positive brake torque and stoichiometric operation were possible.

A local range-restriction boundary model was also fitted for spark advance S as a function of the global variables N, L, ICP, and ECP using a RBF model type.

**Generation of Optimal Survey Calibration**

After completing the boundary-modeling step, a Levenberg-Marquardt nonlinear constrained optimization algorithm[8] was used to generate optimal calibration tables for S, ICP, and ECP based on the survey models for brake torque, residual fraction, and brake torque boundary. The first step in the optimization process is presented below:

- Find maximum brake torque at each operating point in Figure 2 where possible, subject to the constraint that the residual fraction must be less than 20%, and that the solution must lie within the boundary model. Allow 1 Nm of torque to be lost in the interest of gaining 2.5% residual fraction for low NOx emissions.

Equation 2 below shows the objective function used for the first phase of optimization.

$$Objective = TQ + 0.4RF \tag{EQ. 2}$$

Where RF is the cylinder residual fraction measured at IVC.

The second step in the optimization process is presented below:

- For each feasible optimum above, re-optimize by maximizing the sum of all feasible objective values corresponding to the operating points in Figure 2, subject to the constraints above, as well as additional table-smoothness constraints on the resulting S, ICP, and ECP calibration tables

Equation 3 below shows the objective function used for the second phase of optimization.

$$Objective = \sum_{OP} (TQ_{OP} + 0.4RF_{OP}) \tag{EQ. 3}$$

Where OP is an index to the list of feasible Figure 2 operating points found in the first phase of optimization.

The table smoothness (gradient) constraints for the optimal calibrations are shown below in Table 3.

Factor Name	RPM Gradient	Load Gradient
S	+/- 7/500 DegBTDC/RPM	+/-7/0.1 DegBTDC
ICP	+/- 7/500 DegCrank/RPM	+/-7/0.1 DegCrank
ECP	+/- 7/500 DegCrank/RPM	+/-7/0.1 DegCrank

Table 3. Optimization Table Smoothness Constraints

Figures 12, 13, and 14 show visual representations of the optimal survey calibration results for S, ICP, and ECP respectively. As expected, the calibrations shown in Figures 12-14 do not have the fine shape features and trends expected in a well-developed DIVCP calibration due to the fact that they are based on a small survey test data-set.

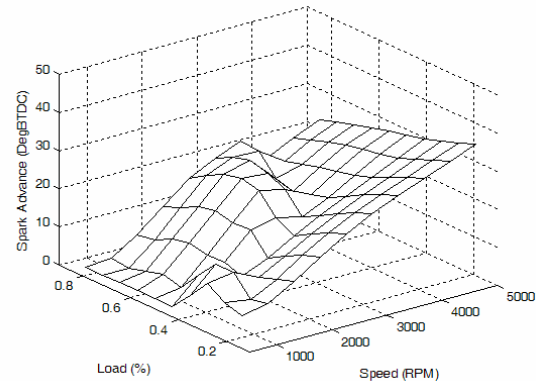


Figure 12. Survey Spark Advance Calibration Table

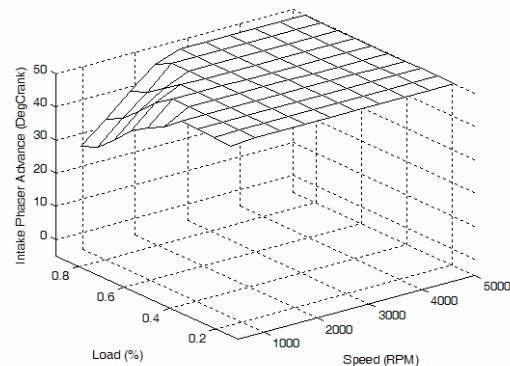


Figure 13. Survey Intake Phaser Advance Calibration Table

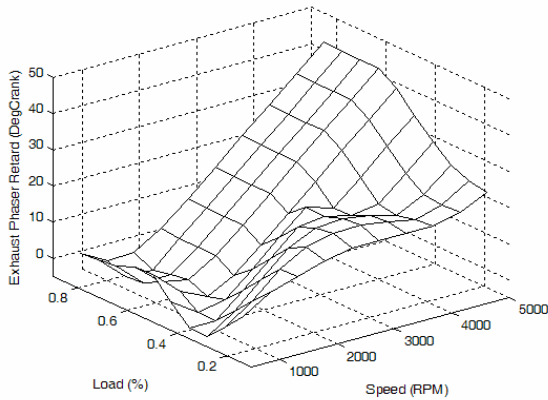


Figure 14. Survey Exhaust Phaser Retard Calibration Table

Global Model	Centers	Kernel Type
$A_0$	23	Wendlands
$A_1$	23	Wendlands
$A_2$	25	Wendlands
$A_3$	25	Wendlands

Table 4. DoE 1 Global Model Characteristics

### Augmented Test Designs

After completing the Survey Calibration Development Process shown in Figure 3, The Augmented Calibration Development Process was executed to produce additional optimization table sets based on increasing numbers of DoE test-points. Five additional DoE test-plans were generated by progressive augmentation by adding Sobol Sequence space-fill points to the original 32 point survey space-fill, and then applying the survey boundary model of Figure 11 to remove out-of-bound points. In addition to the existing survey test plan, test plans containing 96, 173, 250, 329, and 406 torque/spark sweep points were generated. Figures 15 through 19 show the pair wise view of progressive DoE tests 1 through 5 respectively.

### Augmented Test Execution

After completing the augmented DoE designs, test data were generated from the parallel computing cluster discussed previously. The 406 torque/spark sweeps of the augmented DoE designs were executed in 5hrs of computation time.

### Statistical Modeling of Augmented Test Data

The modeling procedure described previously in the survey modeling section was executed on the test data of the augmented DoE designs. Tables 4-8 below summarize the characteristics of the 2<sup>nd</sup> order hybrid RBF global augmented model regressions. Since more data points were available than in the survey test, it was generally possible to use more RBF centers than were used in the survey modeling. Outliers from local torque/spark sweep fits were retained from one augmentation to the next for consistency.

Residual fraction modeling was carried out with the same cubic RBF model form and number of centers for the augmented data sets as was used for the survey test.

Global Model	Centers	Kernel Type
$A_0$	35	Logistic
$A_1$	30	Wendlands
$A_2$	32	Gaussian
$A_3$	32	Reciprocal Multiquadric

Table 5. DoE 2 Global Model Characteristics

Global Model	Centers	Kernel Type
$A_0$	34	Reciprocal Multiquadric
$A_1$	35	Cubic
$A_2$	25	Wendlands
$A_3$	21	Wendlands

Table 6. DoE 3 Global Model Characteristics

Global Model	Centers	Kernel Type
$A_0$	54	Gaussian
$A_1$	39	Wendlands
$A_2$	26	Thinplate
$A_3$	40	Reciprocal Multiquadric

Table 7. DoE 4 Global Model Characteristics

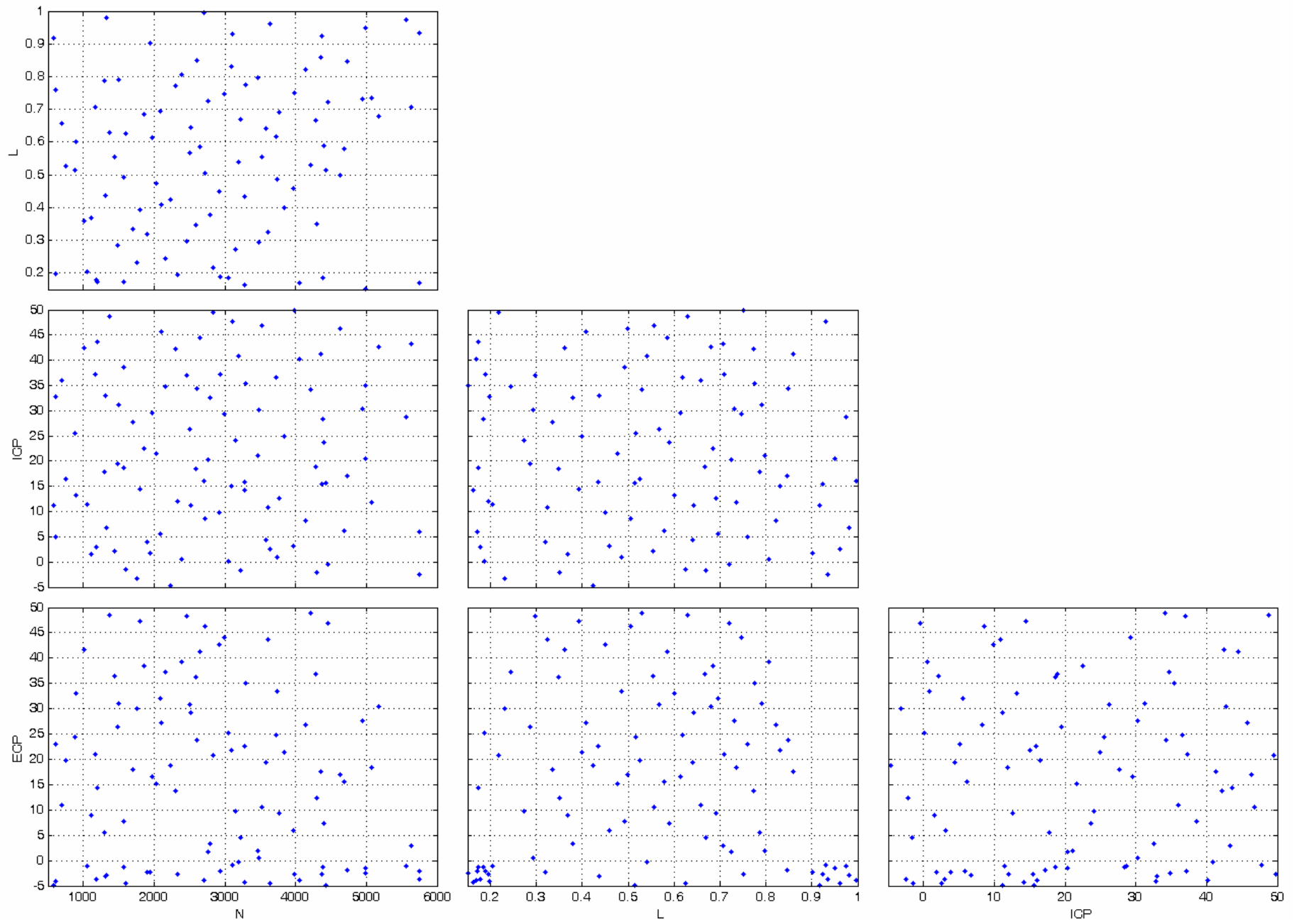


Figure 15. DoE Augmentation 1, 96 Points

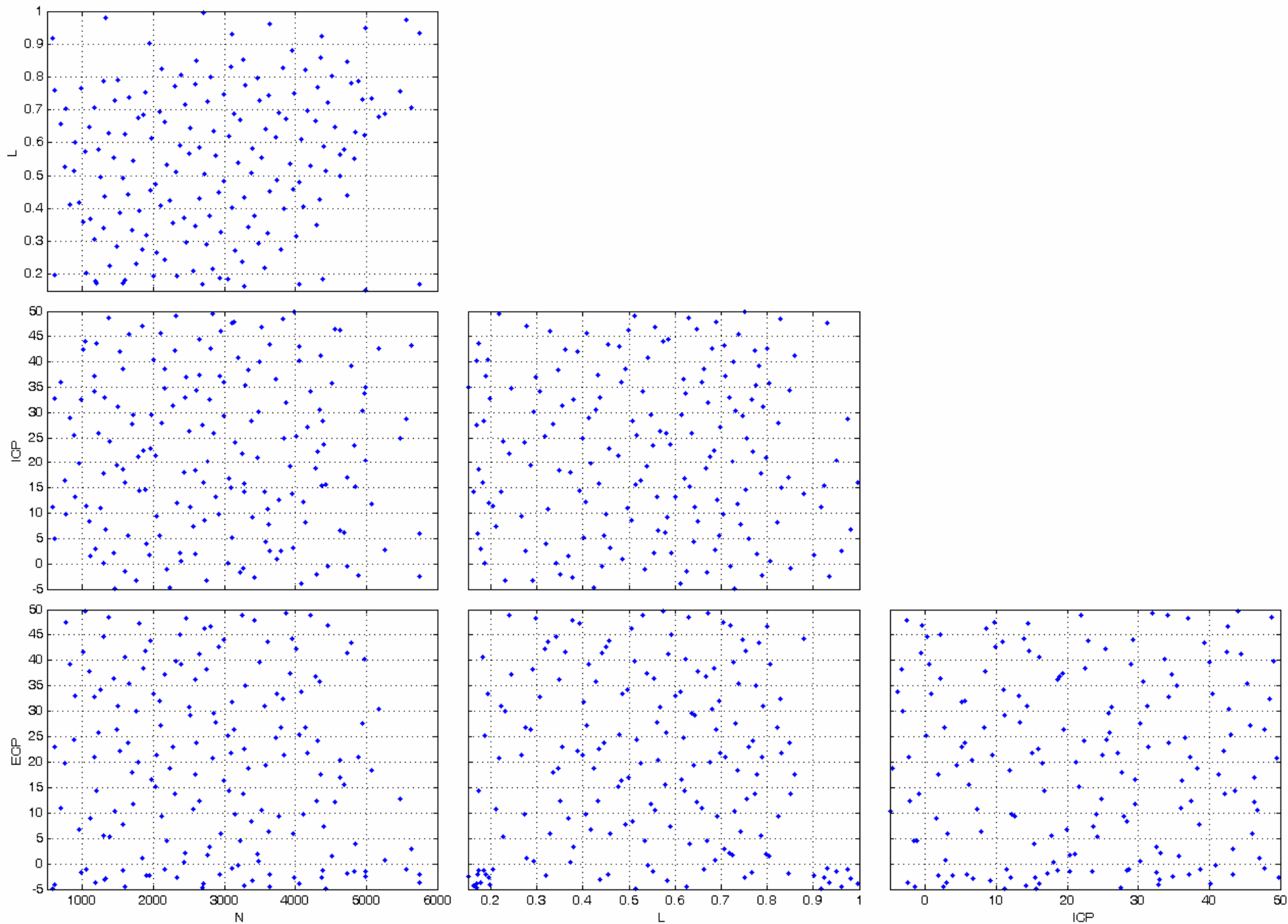


Figure 16. DoE Augmentation 2, 173 Points

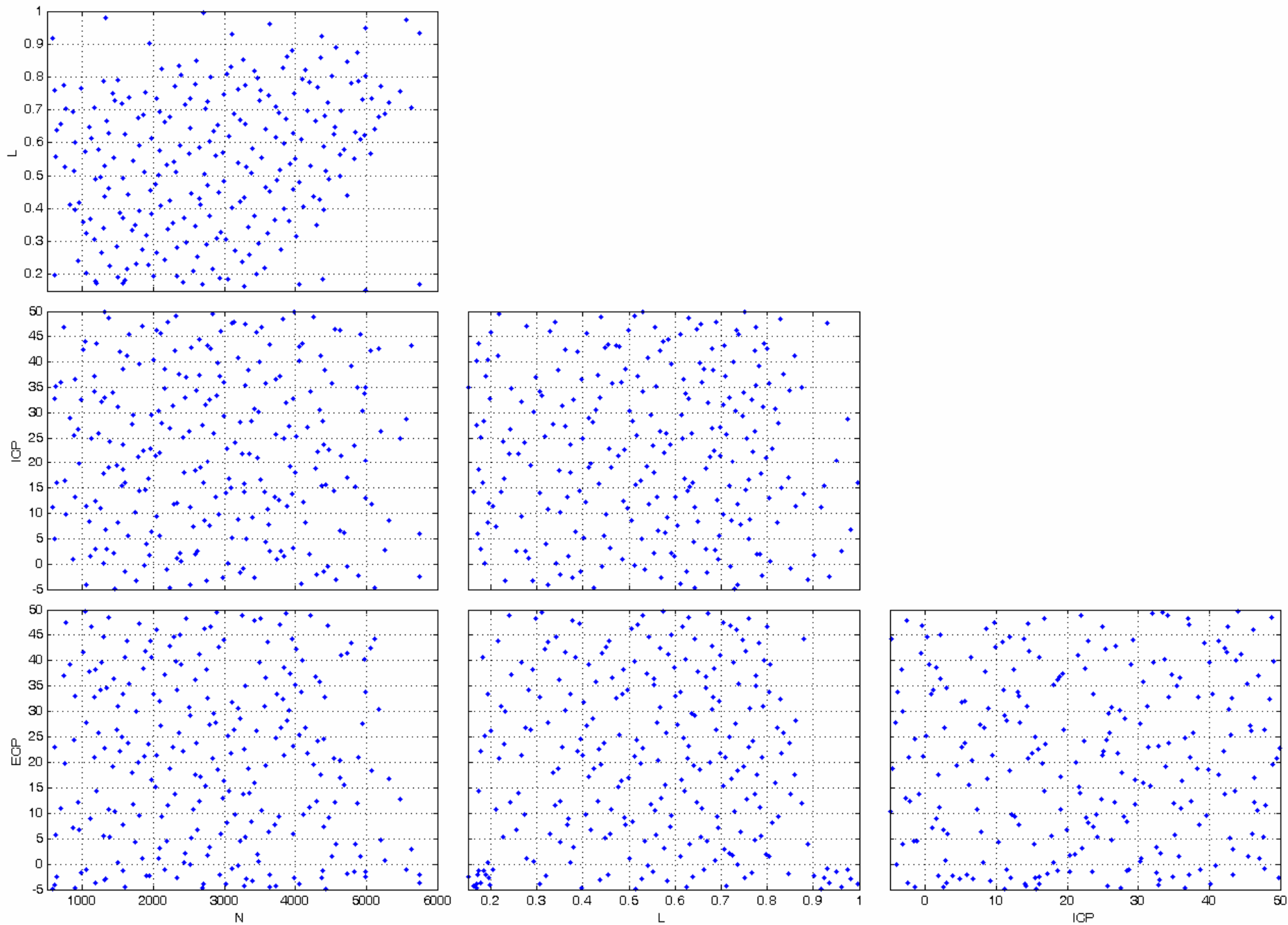


Figure 17. DoE Augmentation 3, 250 Points

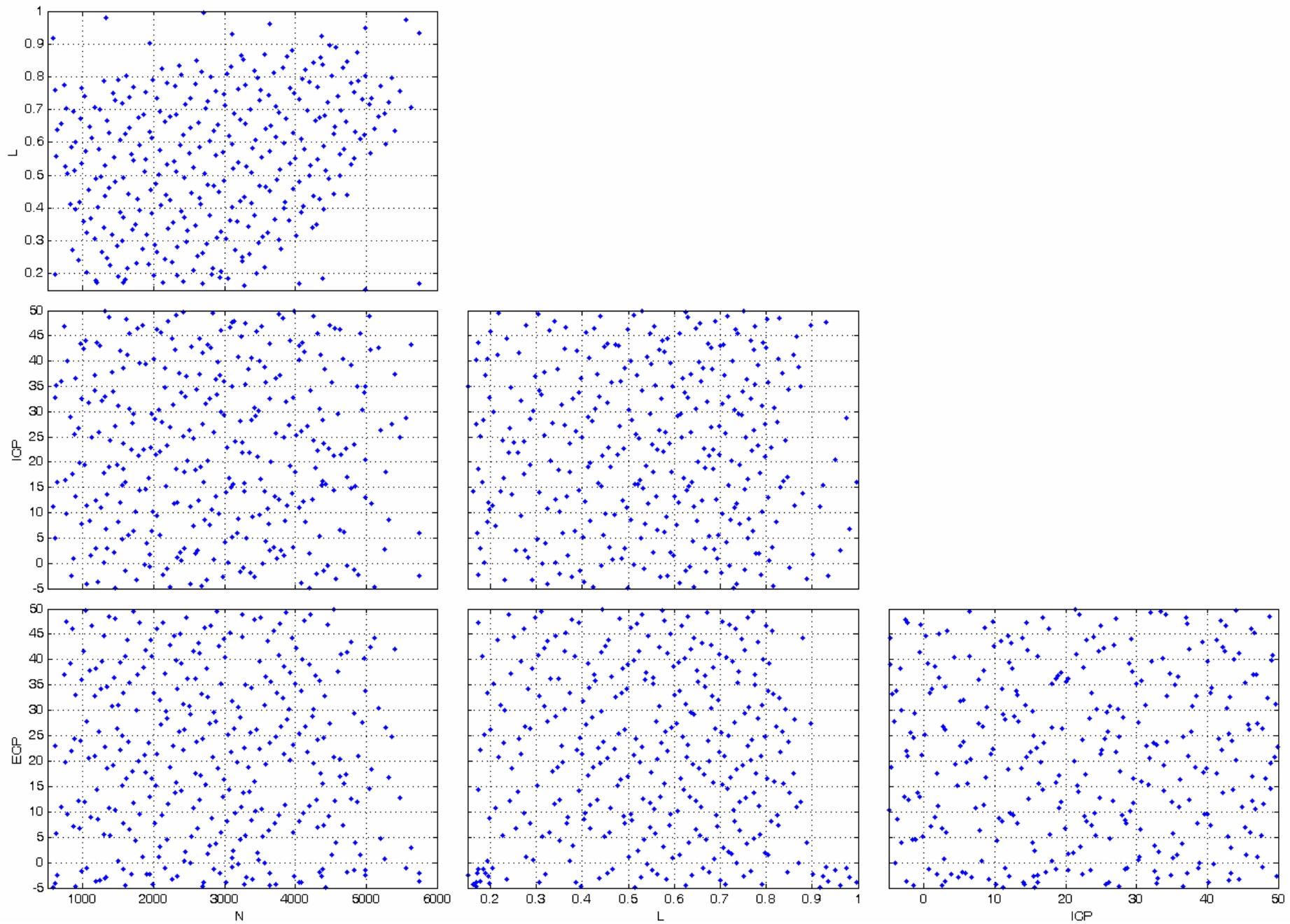


Figure 18. DoE Augmentation 4, 329 Points

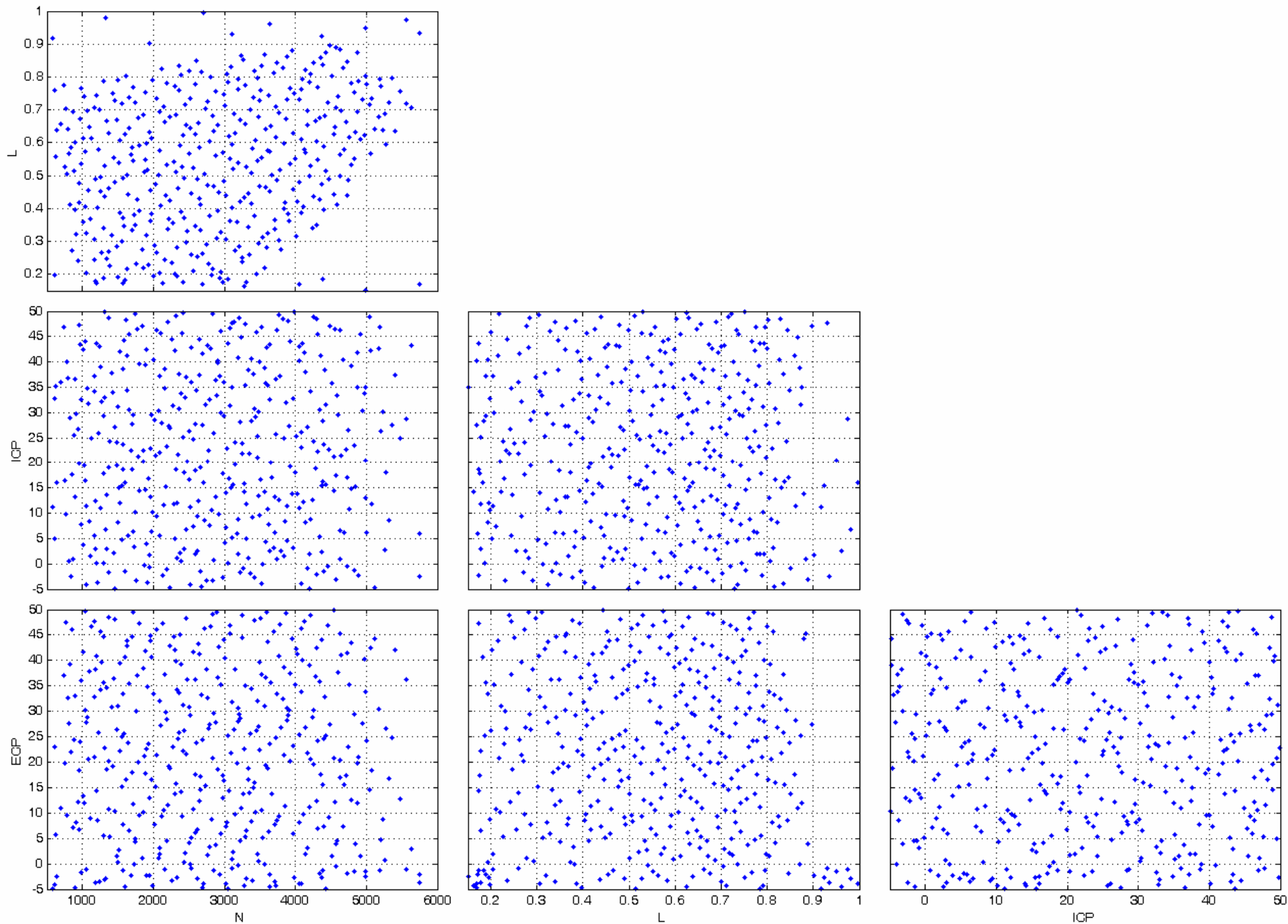


Figure 19. DoE Augmentation 5, 406 Points

Global Model	Centers	Kernel Type
$A_0$	69	Wendlands
$A_1$	60	Reciprocal Multiquadric
$A_2$	52	Wendlands
$A_3$	74	Multiquadric

Table 8. DoE 5 Global Model Characteristics

Figures 20-24 below show the frequency distribution of the residual differences between predicted and measured torque, and predicted and measured residual fraction for augmented DoE models 1-5 respectively.

The torque residual distributions show that with the production-intent modeling approach in this paper, brake torque cannot be expected to be modeled more accurately than about  $\pm 2.5$  Nm for any given measurement point, regardless of the amount of data collected. In like manner, residual error distribution in residual fraction show that residual fraction cannot be expected to be modeled more accurately than about  $\pm 1.5\%$ , using a cubic RBF form, regardless of the amount of data collected.

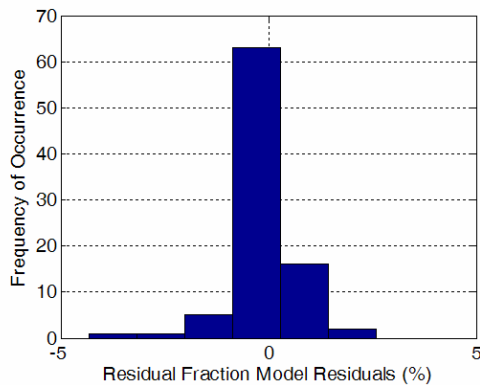
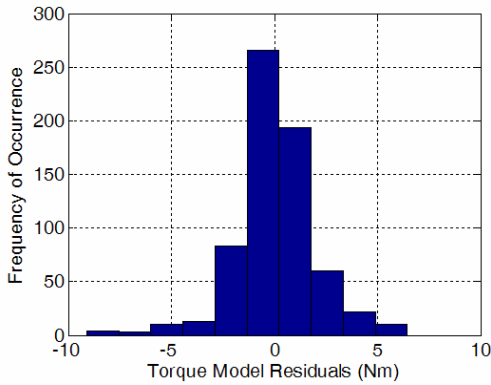


Figure 20. DoE 1 Model Residual Distributions

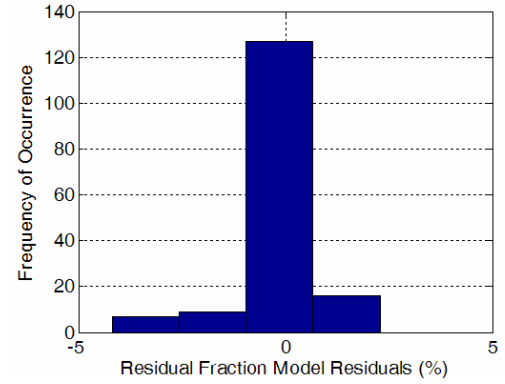
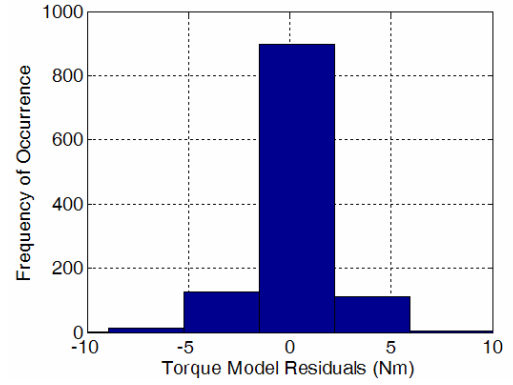


Figure 21. DoE 2 Model Residual Distributions

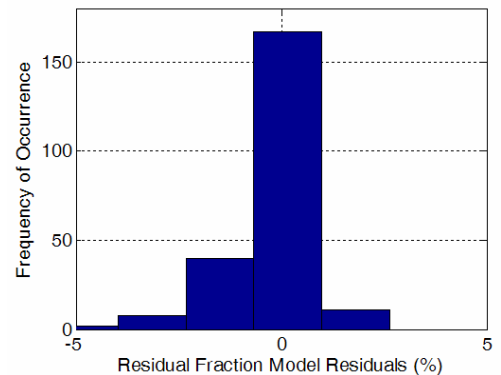
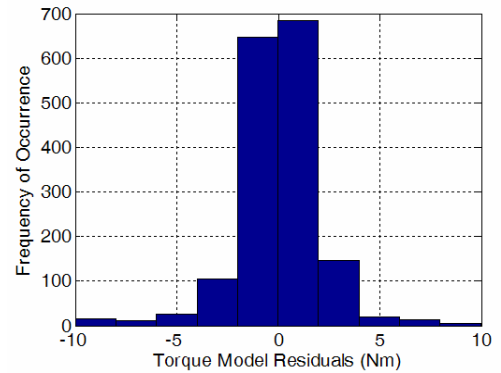


Figure 22. DoE 3 Model Residual Distributions

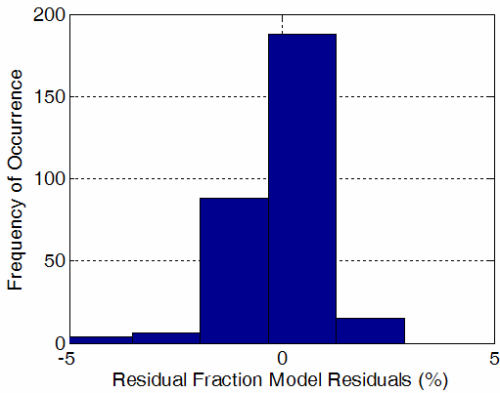
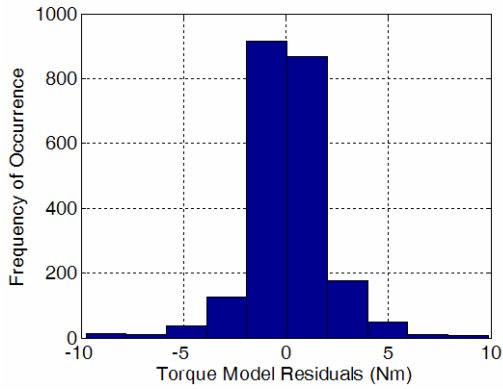


Figure 23. DoE 4 Model Residual Distributions

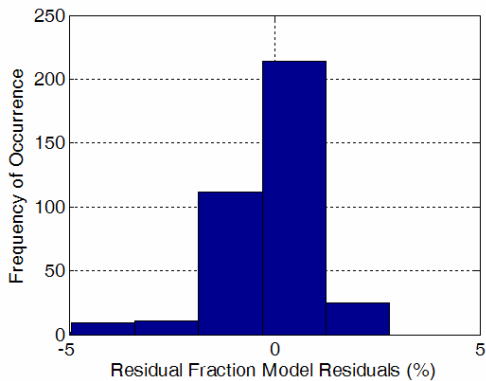
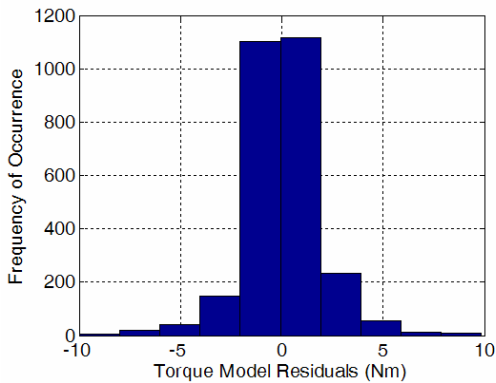


Figure 24. DoE 5 Model Residual Distributions

### Boundary Modeling of Augmented Test Data

After each DoE augmentation, the convex hull and local range survey boundary modeling procedure presented previously was re-applied, with very similar results to those shown in Figure 11, since the augmented points were collected within the original survey boundary to begin with.

### Generation of Optimal Survey Calibration

The Levenberg-Marquardt nonlinear constrained optimization process used previously in survey calibration optimization was re-applied to each DoE augmentation and modeling iteration. Figures 25-29 below show the optimal calibration tables related to DoE augmentations 1-5 respectively.

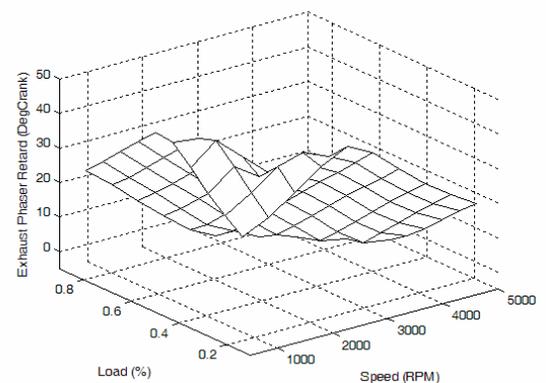
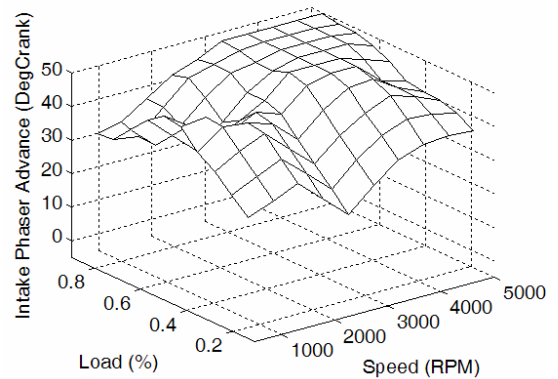
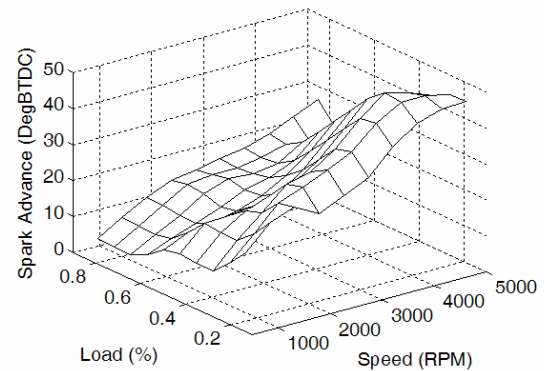


Figure 25. Optimal Calibrations Associated With DoE 1

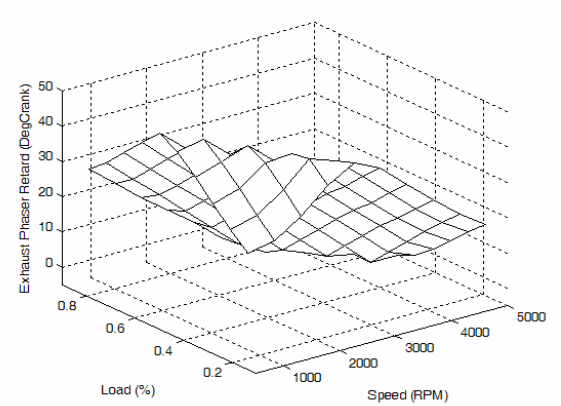
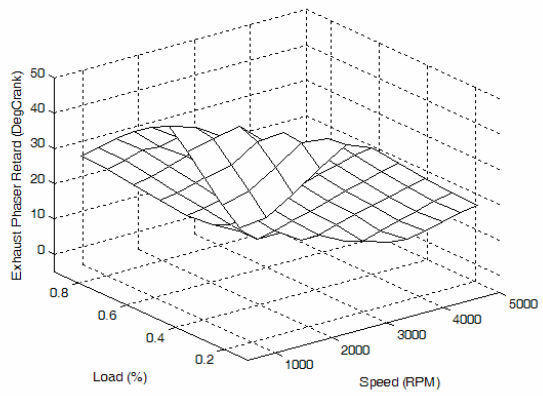
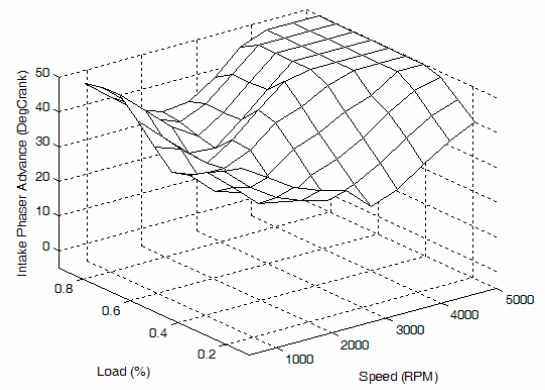
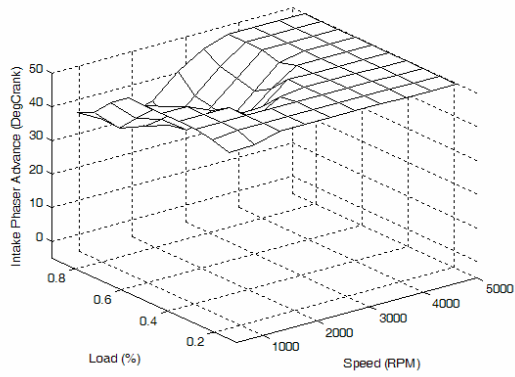
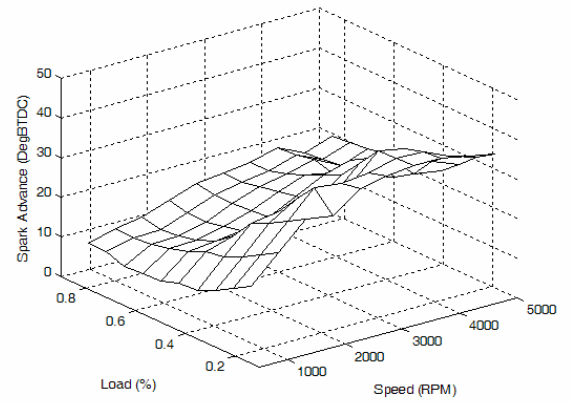
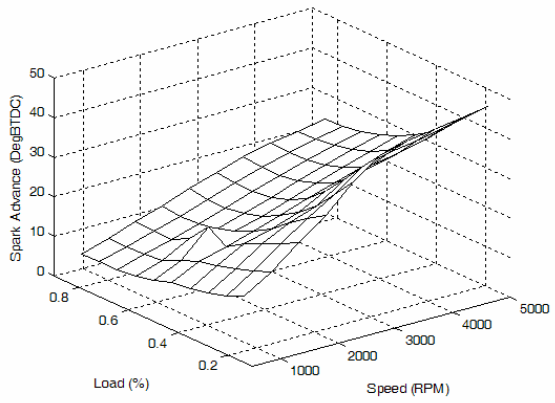


Figure 26. Optimal Calibrations Associated With DoE 2

Figure 27. Optimal Calibrations Associated With DoE 3

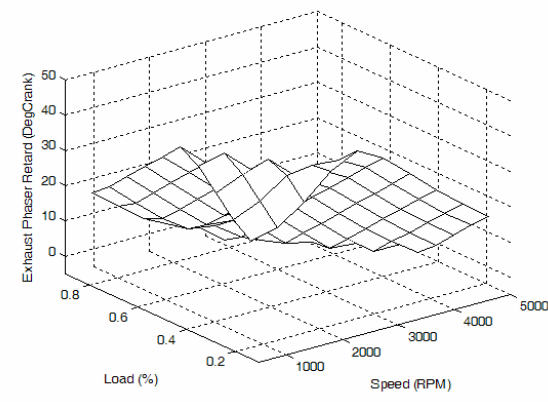
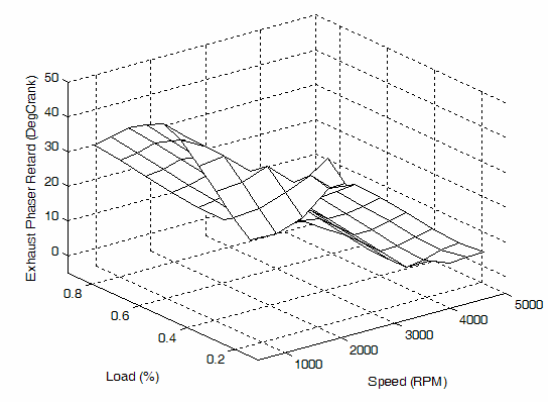
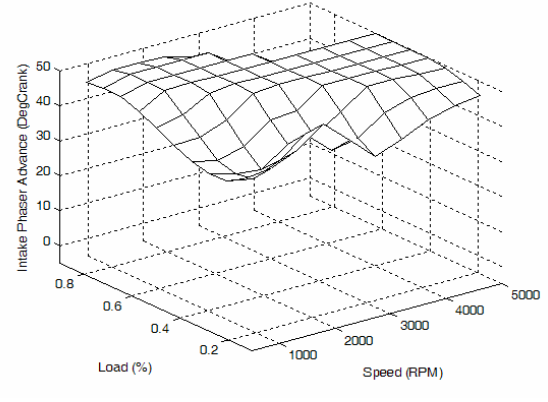
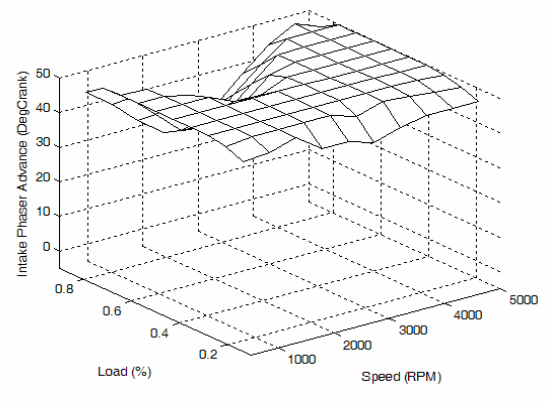
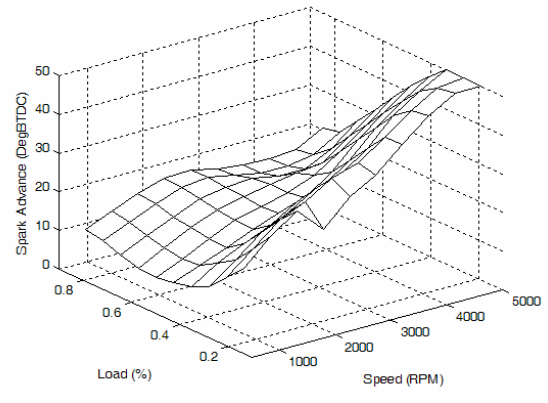
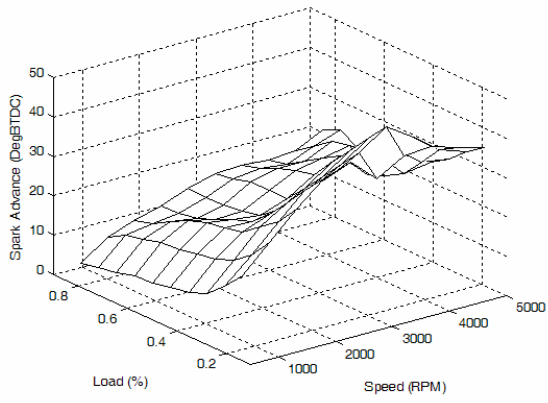


Figure 28. Optimal Calibrations Associated With DoE 4

Figure 29. Optimal Calibrations Associated With DoE 5

### Operating Point DoE Test Design

Comparing the calibrations in Figures 25-29 to the survey calibrations in Figures 12-14, it is clear that the shapes and trends of the calibrations related to the augmented DoE tests are significantly different from those of the survey test, most likely due to the fact that the survey did not have sufficient points to develop a good calibration.

Smaller calibration variations between calibrations related to the larger augmented DoE designs in Figures 25-29 are most likely attributable to modeling process variations from the best-fit AICc model choices presented in tables 4-8, based on the idea that the calibration shapes and trends should converge as DoE experiment size increases.

### **Exhaustive Calibration Process**

The Exhaustive Calibration Development Process in Figure 3 was executed In addition to the more cost-feasible production-intent survey and augmented DoE tests shown previously, in order to establish a reference optimal calibration that would represent the best effort at finding truly optimal results.

To insure dense blanket-coverage of the engine factor space in Table 1, a 100 point Sobol Sequence DoE was designed in ICP/ECP cam factor-space and tested at every speed/load point shown in Figure 2. For each of the 100 cam factor-space points, an exhaustive spark-sweep was executed from 0 to 50 DegBTDC in 1 degree increments. The total number of torque/spark sweeps in the exhaustive DoE test plan was therefore 10,000 , corresponding to 510,000 total measurements. Figure 30 below shows the cam factor-space Sobol DoE design applied at each speed/load operating point.

### Exhaustive Test Execution

After completing the exhaustive DoE design, the parallel computing cluster presented previously in the Survey Test Execution section was used to generate the exhaustive DoE data. 510,000 data-points were completed by the 16 PC cluster in 10 days of computation time.

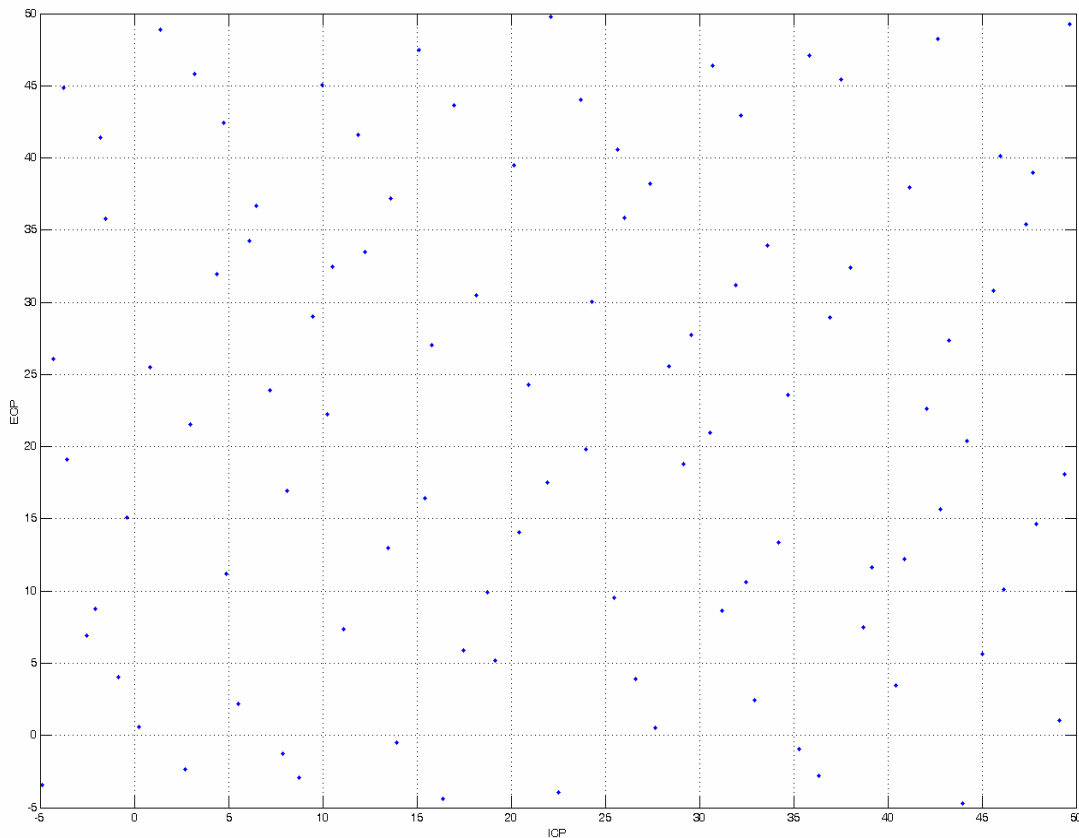


Figure 30. Operating Point Sobol DoE in Cam Factor-Space

## Statistical Modeling of Exhaustive Test Data

After collection of the exhaustive test data, each of the 10,000 torque/spark sweeps were pre-filtered to include only the data corresponding to the location of peak torque, resulting in peak torque settings to 1 DegBTDC spark advance resolution for 100 combinations of cam factor-space settings at each of 100 speed/load points.

After pre-filtering, cubic RBF response models and convex hull boundary models were fitted automatically for torque and residual fraction at each speed/load operating point, resulting in 100 torque models, 100 residual fraction models, 100 spark advance models, and 100 boundary models. The cubic RBF response models were built with between 5 and 10 centers, or up to approximately 10% of the data points gathered at each speed/load point in cam factor-space.

## Generation of Optimal Exhaustive Calibration

Optimal exhaustive calibration tables were generated from the exhaustive models using the same calibration optimization procedure as presented previously in the Generation of Optimal Survey Calibration, except that no spark advance table gradient was imposed.

Figure 31 shows the optimal calibrations generated by the exhaustive calibration optimization process. The shapes and trends of the previous augmented DoE calibrations are similar to the exhaustive calibration, but not very similar to the Survey DoE, which was derived from the smallest number of test points.

## Determination of Minimum DoE Size

The minimum cost-feasible DoE size was determined by comparing the brake torque measured in calibration validation testing between the exhaustive calibration and the other six cost-feasible calibrations. Figures 32-37 show the residual differences between the calibrations, measured brake torque, measured residual fraction, and predicted torque for each cost-feasible calibration. Figures 32-37 show that as DoE size increases above the survey size of 52 spark sweeps, the difference between the cost-feasible torque production and the exhaustive torque production converge, except for a few points at the load extremes of the speed/load operating points. A similar pattern of convergence occurred with residual fraction and torque prediction error. Torque prediction error is the difference between the torque estimated by the calibration process and the torque measured in the validation process.

Despite the convergence in torque production between the exhaustive and cost-effective calibration approaches, the calibration settings that drive the torque

production results can vary fairly significantly, with different combinations of S, ICP, and ECP producing similar torque results.

As an alternative to viewing the differences between calibrations in terms of operating-point location, Figure 38 shows minimum (torque loss), median negative residuals, and maximum (torque gain) torque residuals relative to the exhaustive results across all operating points, also indicating that DoE sizes above about 52 points show diminishing returns in torque production.

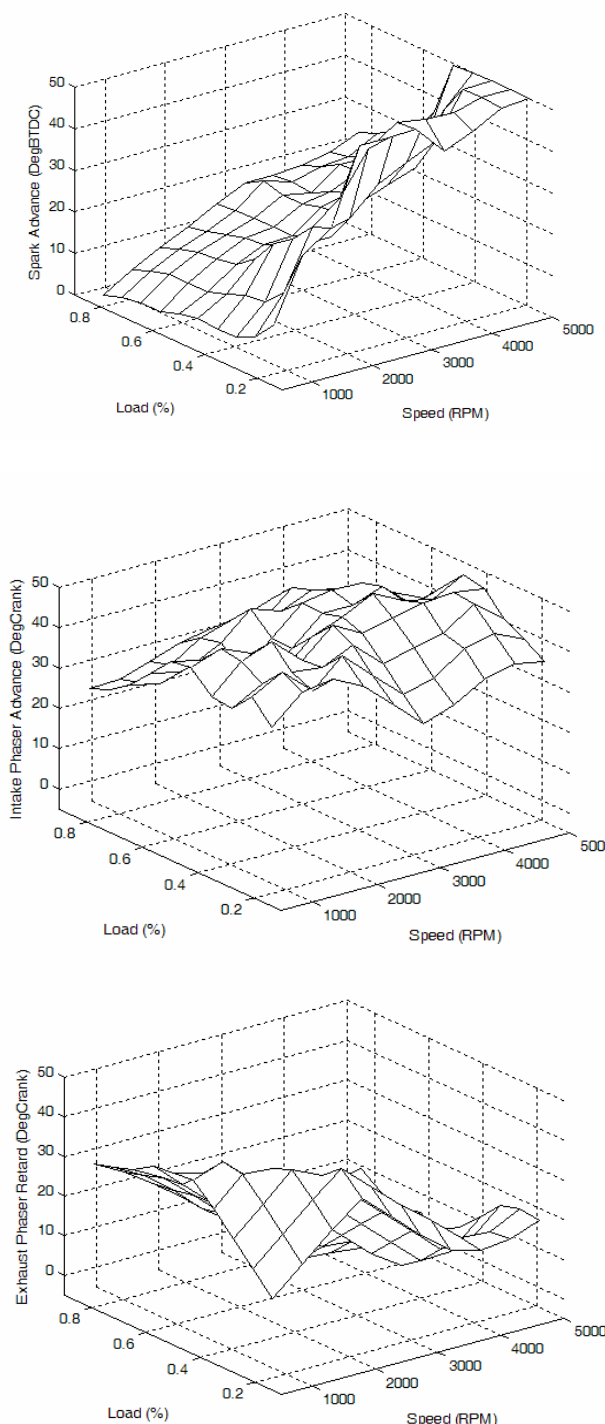


Figure 31. Optimal Calibrations Associated With Exhaustive DoE

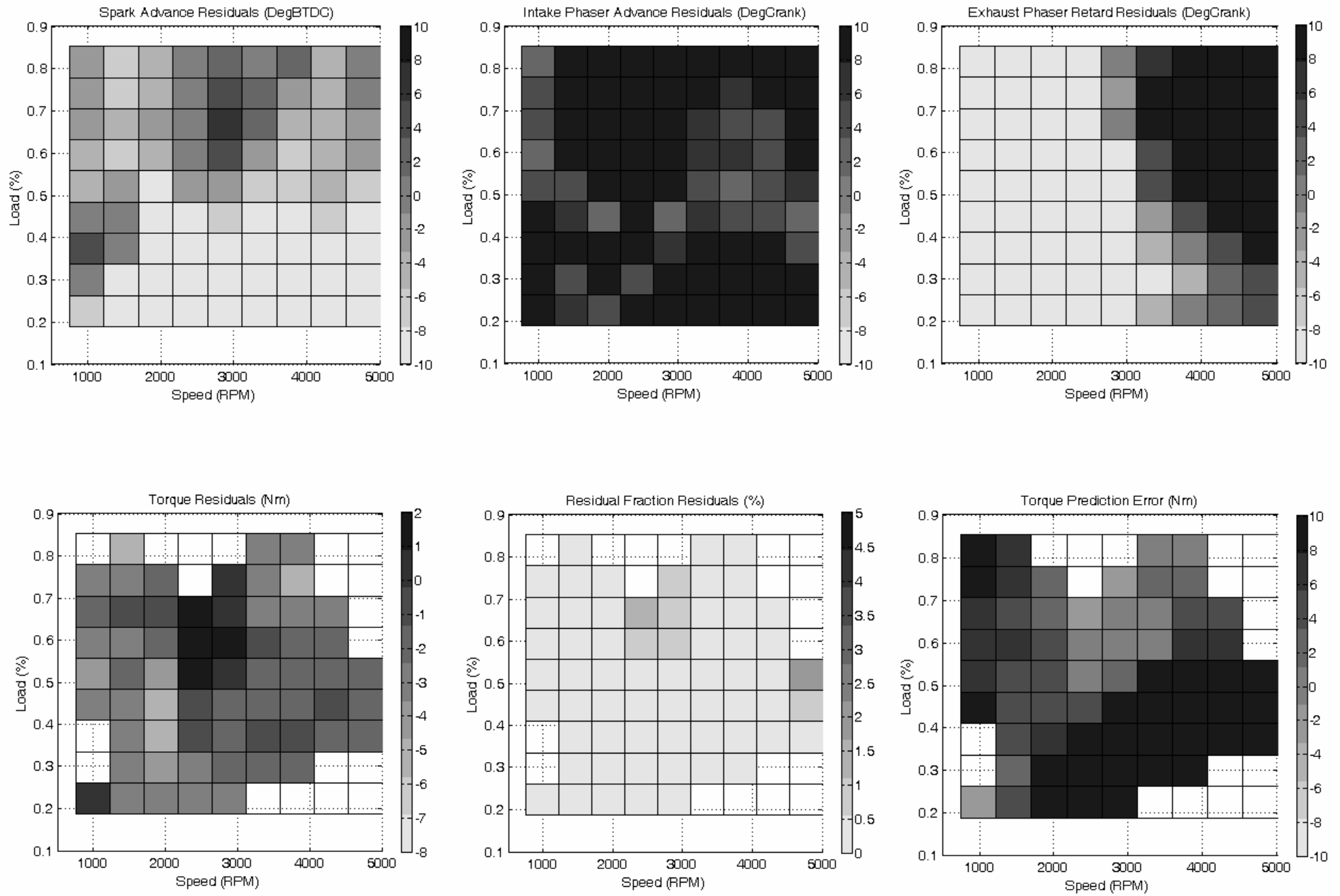


Figure 32. Survey Calibration, Measured Torque, Measured Residual Fraction, and Predicted Torque Residuals Relative to Exhaustive Calibration

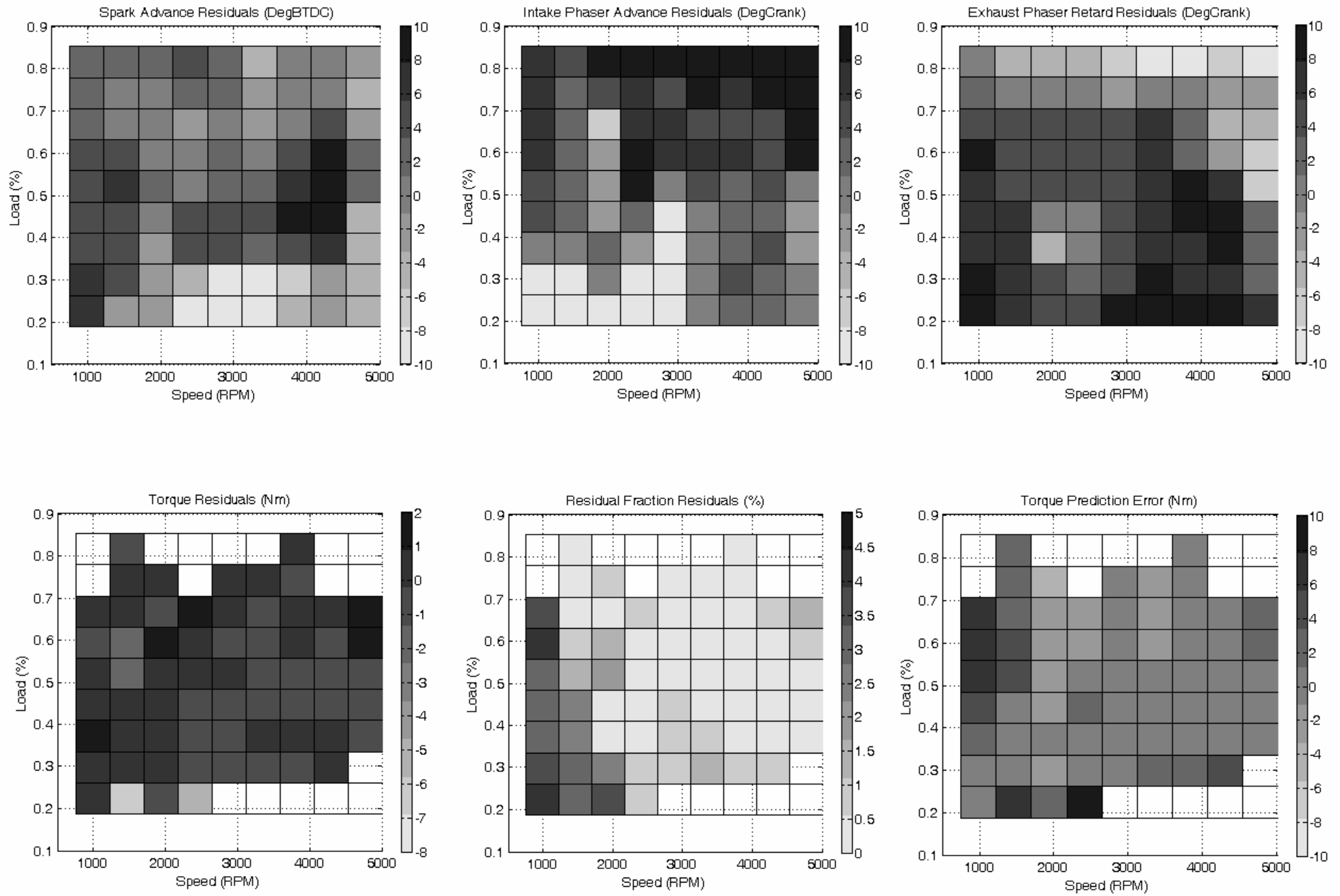


Figure 33. DoE 1 Calibration, Measured Torque, Measured Residual Fraction, and Predicted Torque Residuals Relative to Exhaustive Calibration

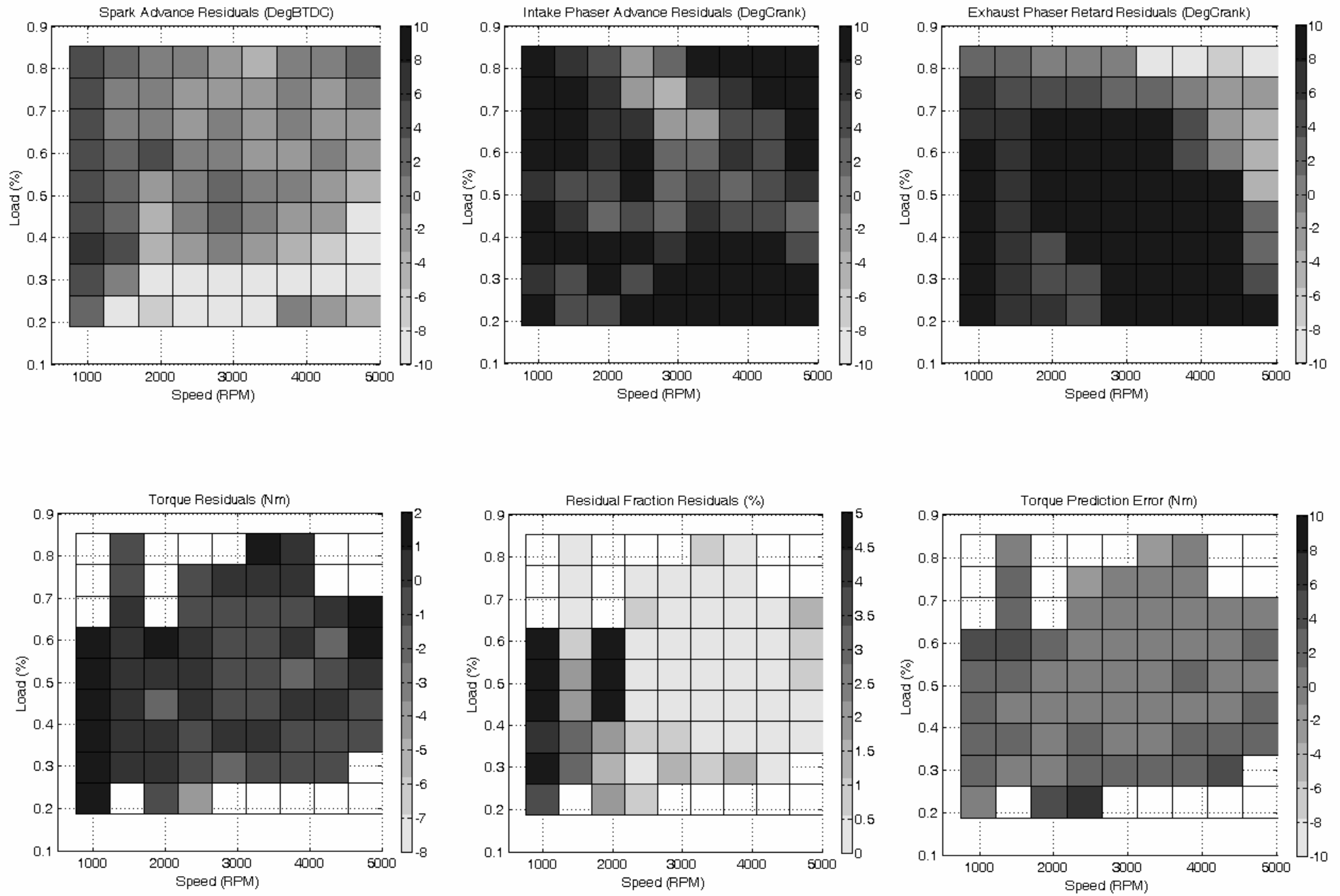


Figure 34. DoE 2 Calibration, Measured Torque, Measured Residual Fraction, and Predicted Torque Residuals Relative to Exhaustive Calibration

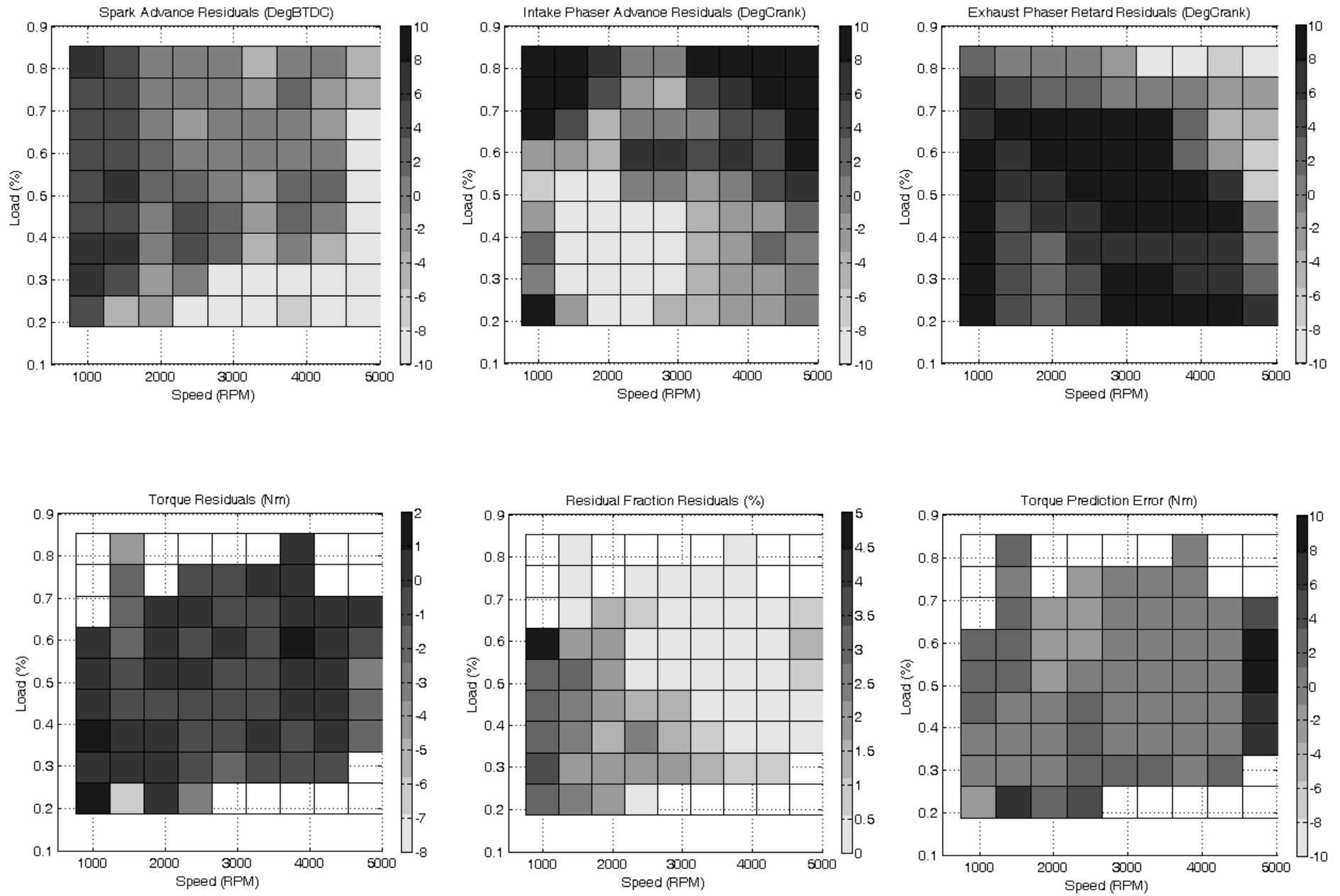


Figure 35. DoE 3 Calibration, Measured Torque, Measured Residual Fraction, and Predicted Torque Residuals Relative to Exhaustive Calibration

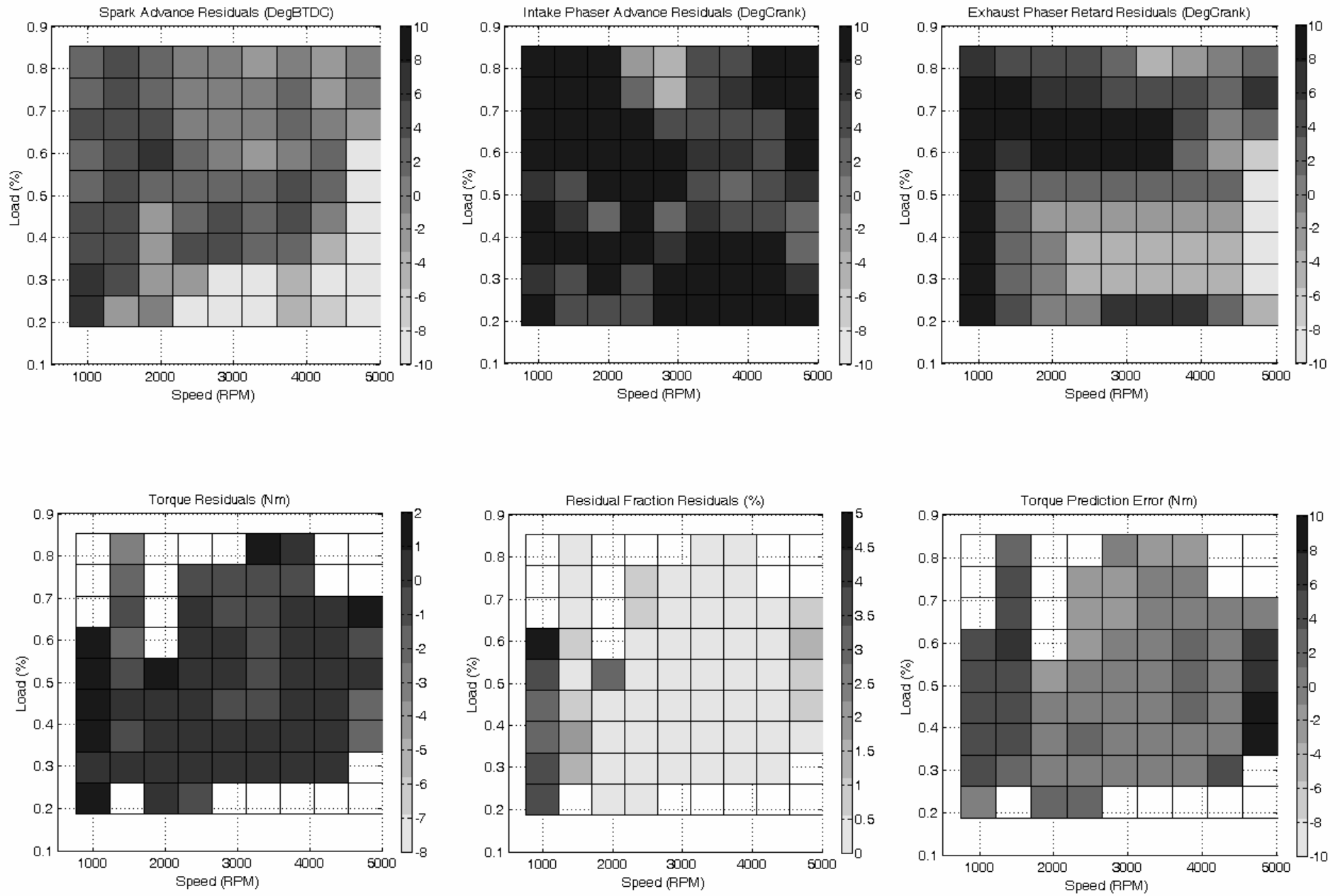


Figure 36. DoE 4 Calibration, Measured Torque, Measured Residual Fraction, and Predicted Torque Residuals Relative to Exhaustive Calibration

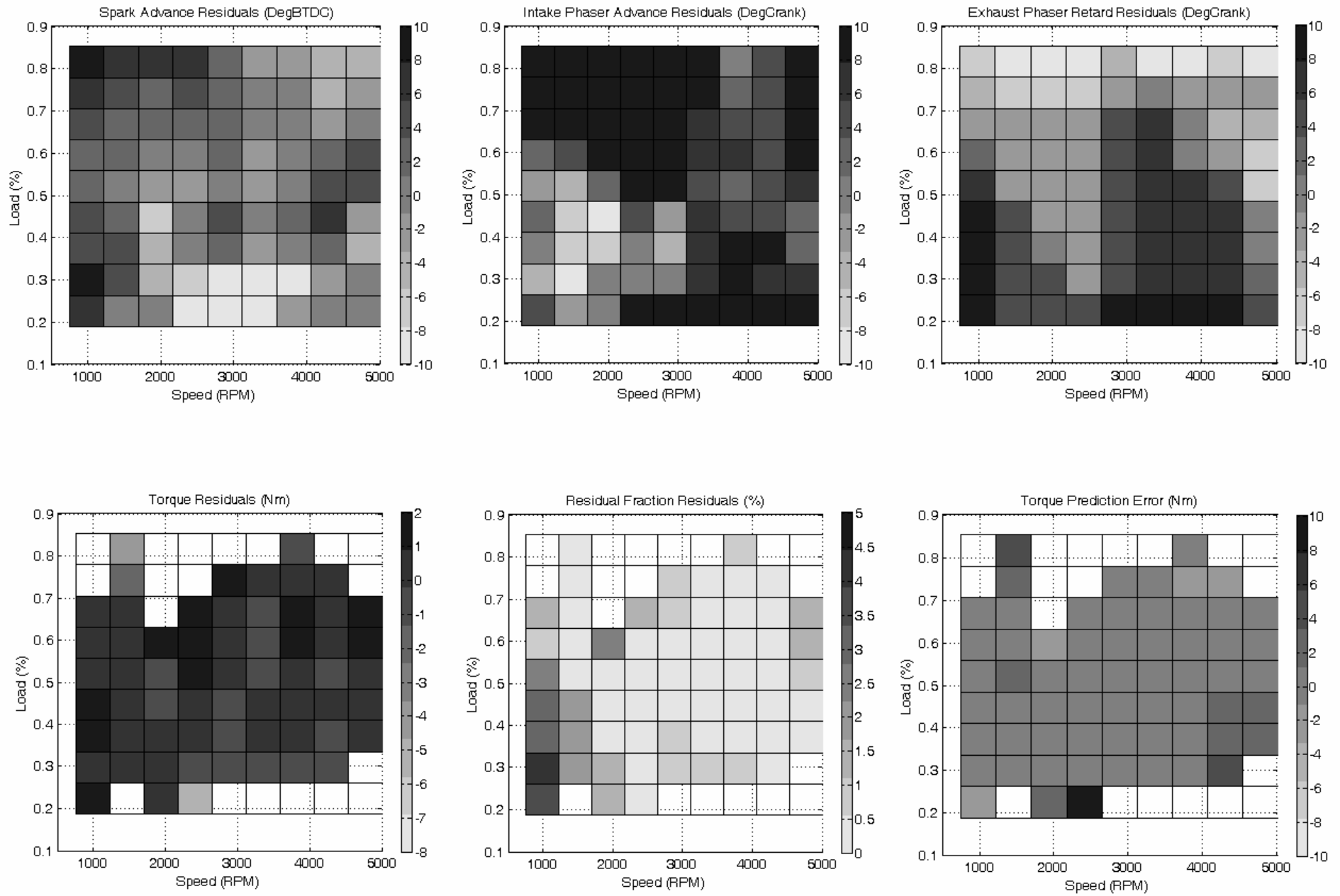


Figure 37. DoE 5 Calibration, Measured Torque, Measured Residual Fraction, and Predicted Torque Residuals Relative to Exhaustive Calibration

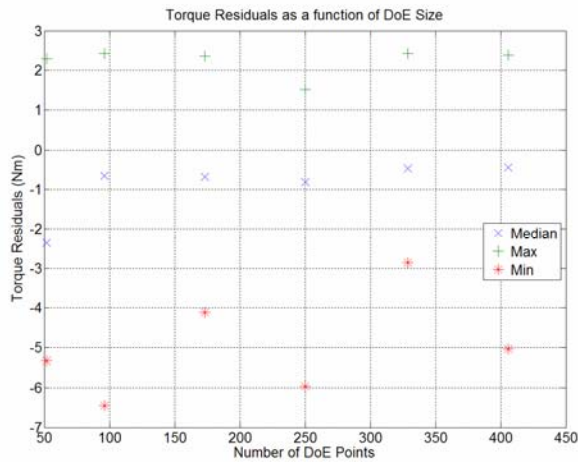


Figure 38. Minimum, Median Loss, and Maximum Torque Residuals

Figure 38 shows that in some cases the cost-feasible calibration approaches out-performed the exhaustive calibration by approximately 2.5 Nm, most likely due to the fact that the exhaustive approach was not completely exhaustive in terms of cam factor-space, and that it still required some modeling of the data, which in turn resulted in small modeling errors. The minimum residuals represent the speed/load locations of worst-case torque loss for cost-feasible calibrations, and indicate that the considerable variation caused by variable model types, gaps in DoE coverage, and boundary model fits are unavoidable regardless of DoE size. There is, however a slight decreasing trend in worst-case minimum residuals as DoE size increases, but the decrease is not likely to be worth the extra cost in testing. The median negative residuals in Figure 38 show that calibration results improve substantially somewhere between 52 and 100 spark-sweeps, making 100 spark sweeps a reasonable DoE size choice for an SI DIVCP engine of the type modeled in this paper.

## CONCLUSIONS

A process for objectively determining the cost-feasible minimum number of torque/spark sweeps to optimally calibrate a SI DIVCP engine was designed, developed, and implemented based on a GT-POWER engine model configured with predictive combustion capability.

An analysis of the process outputs shows that approximately 100 torque/spark-sweeps are required to optimally calibrate an SI DIVCP engine, given the assumption that the model and engine architecture used in this paper are relevant to a production application of interest.

## REFERENCES

1. Baker, R., Daby, E., "Engine Mapping Methodology", SAE Paper 770077, 1977.
2. Wu, B., Filipi, Z., Prucka, R., Kramer, D., Ohi, G. "Cam-phasing Optimization Using Artificial Neural Networks as Surrogate Models - Fuel Consumption and NOx Emissions", SAE Paper 2006-01-1512, 2006.
3. Carter, N., Gabler, R., "A Model Based Calibration Process for Robust Optimal Cam Position Selection Under all Engine Operating Conditions", SAE Paper 2008-01-1366, 2008.
4. Bratley, P., Fox, B., "ALGORITHM 659 Implementing Sobol's Quasirandom Sequence Generator." ACM Transactions on Mathematical Software. Vol. 14, No. 1, 1988, pp. 88-100
5. Chen, S., Chng, E., Alkadhimi, "Regularized Orthogonal Least Squares Algorithm for Constructing Radial Basis Function Networks", Int J. Control, 1996, Vol. 64, No. 5, pp. 829-837.
6. Burnham, K., Anderson, D., "Model Selection and Multimodel Inference" , Second Edition, Springer-Verlag, 2002
7. Barber, C., Dobkin, D., Huhdanpaa, H., "The Quickhull algorithm for convex hulls," ACM Trans. on Mathematical Software, 22(4):469-483, Dec 1996
8. Levenberg, K., "A Method for the Solution of Certain Problems in Least Squares," Quart. Appl. Math. Vol. 2, pp 164-168, 1944.

## ACKNOWLEDGEMENTS

The author would like to thank Ian Noell, Paul Kerr-Delworth, Richard Lang, and Tish Sheridan of the Model-Based Calibration Toolbox™ team for the steadfast support and theoretical guidance needed to complete the work in this paper. Thanks are also due to David Sampson of the Consulting team for determining and clarifying industry problems related to SI DIVCP calibration development over the past 8 years. Since the work in this paper would not have been possible without the use of well-developed engine simulation models, special thanks go to the talented engineers at Gamma Technologies for their support and guidance during engine model development.